### Evaluation of neurotoxicity

The severity of neurotoxicity was assessed both electrophysiologically and histologically. Under intraperitoneal ketamine anaesthesia (40 mg kg$^{-1}$), rats were given a single i.v. injection of PTX (7.5 mg kg$^{-1}$), NK105 (a PTX-equivalent dose of 7.5 mg kg$^{-1}$), or 5% glucose weekly for 6 weeks. All the solutions were administered through the jugular vein exposed via a small incision in the neck. Electrophysiological measurements were conducted 1 day before the first dosing and on day 6 after the final dosing. For electrophysiological recording, rats were anaesthetised by the intraperitoneal injection of pentobarbital 40 mg kg$^{-1}$. Electrical stimuli were given peripherally, and caudal sensory nerve action potentials (caudal SNAPs) were recorded centrally from the tail. The amplitude of each waveform was calculated by measuring the caudal SNAP from the top peak to the bottom peak. Variations in the amplitude after the 6th weekly administration of the solutions were determined.

For light microscopy, rats were killed after electrophysiological recordings. Subsequently, a segment of the sciatic nerve was carefully removed, and embedded in paraffin. Sections (2 $\mu$m thick) were stained with haematoxylin and eosin (H & E) before examination under light microscopy to evaluate the degenerative changes of myelinated nerve fibres.

### Statistical analysis

The data of therapeutic efficacy was expressed as mean $\pm$ s.e.m. The statistical significance of differences in therapeutic efficacy between two administration groups was calculated by means of repeated measures (analysis of variance). The statistical significance of the differences in neurotoxic activity between two administration groups was calculated using the Student's $t$-test on the closed testing procedure. The histopathological impairment was scored in five grades. The statistical significance of the differences in histopathological impairment between two administration groups was calculated using the Wilcoxon's rank-sum test on the closed testing procedure. All data were calculated with software StatView, version 5 (ABACUS Concepts, Berkeley, CA, USA). A value of $P<0.05$ was considered statistically significant.

## RESULTS

### Preparation and characterisation of NK105

To construct NK105 micellar nanoparticles (Figure 1A), block copolymers consisting of PEG and polyaspartate, the so-called PEG polyaspartate described previously (9, 11, 13, 14), were used. PTX was incorporated into polymeric micelles formed by physical entrapment utilising hydrophobic interactions between PTX and the block copolymer polyaspartate chain. After screening of many candidate substances, 4-phenyl-1-butanol was employed for the chemical modification of the polyaspartate block to increase its hydrophobicity. Treating with a condensing agent, 1,3-diisopropylcarbodiimide, the half of carboxyl groups on the polyaspartate, was esterified with 4-phenyl-1-butanol. Molecular weight of the polymers was determined to be approximately 20 000 (PEG block: 12 000; modified polyaspartate block: 8000). NK105 was prepared by facilitating the self-association of NK105 polymers and PTX. NK105 was obtained as a freeze-dried formulation and contained ca. 23% (w w$^{-1}$) of PTX, as determined by reversed-phase liquid chromatography using an ODS column with mobile phase consisting of acetonitrile and water (9 : 11, v v$^{-1}$) and detection of ultraviolet absorbance at 227 nm. Finally, NK105, a PTX-incorporating polymeric micellar nanoparticle formulation with a single and narrow size distribution, was obtained. The weight-average diameter of the nanoparticles was approximately 85 nm ranging from 20 to 430 nm (Figure 1B).

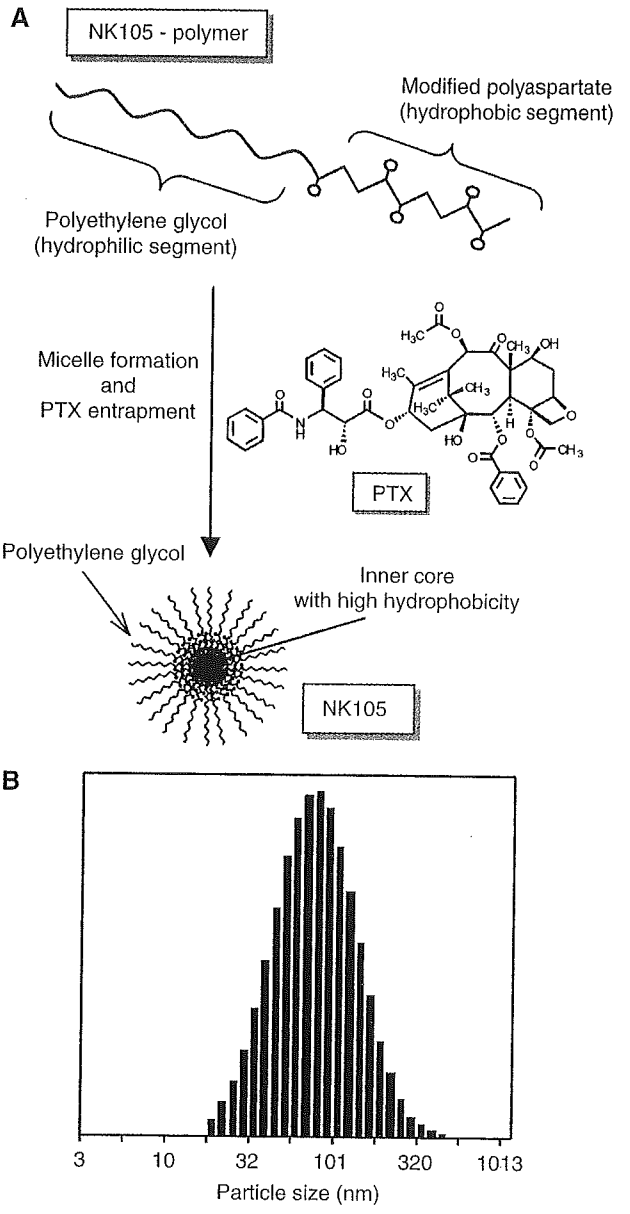


**Figure 1** Preparation and characterisation of NK105. (**A**) The micellar structure of NK105 PTX was incorporated into the inner core of the micelle. (**B**) The size distribution of NK105 measured by the dynamic light scattering method. The mean diameter of an NK105 micelle was 85 nm.

### Pharmacokinetics and pharmacodynamics of NK105

Colon 26-bearing CDF1 mice were given a single i.v. injection of PTX 50 or 100 mg kg$^{-1}$, or of NK105 at an equivalent dose of PTX. Subsequently, the time-course changes in the plasma and tumour levels of PTX were determined in the PTX and NK105 administration groups (Figure 2); furthermore, the pharmacokinetic parameters of each group were also determined (Table 1). NK105 exhibited slower clearance from the plasma than PTX, while NK105 was present in the plasma for up to 72 h after injection; PTX was not detected after 24 h or later of injection. The plasma concentration at 5 min ($C_{5\,min}$) and the area under the curve (AUC) of NK105 were 11–20-fold and 50–86-fold higher for NK105 than for PTX, respectively. Furthermore, the half-life at the terminal phase ($t_{1/2z}$) was 4–6 times longer for NK105 than for

PTX. The maximum concentration ($C_{max}$) and AUC of NK105 in Colon 26 tumours were approximately 3 and 25 times higher for NK105 than for PTX, respectively. NK105 continued to accumulate in the tumours until 72 h after injection. The tumour PTX concentration was higher than 10 $\mu g\,g^{-1}$ even at 72 h after the i.v. injection of NK105 50 and 100 $mg\,kg^{-1}$. On the contrary, the tumour PTX concentrations at 72 h after the i.v. administration of free PTX 50 and 100 $mg\,kg^{-1}$ were below detection limits and less than 0.1 $\mu g\,g^{-1}$, respectively.

### *In vitro* cytotoxicity

NK105 was tested on 12 human tumour cell lines derived from lung, gastric, oesophagus, colon, breast, and ovarian tumours. Similar dose–response curves were noted for PTX and NK105 (data not shown). Furthermore, the $IC_{50}$ values of NK105 were similar to those of PTX at 48 and 72 h, indicating that both NK105 and PTX showed equivalent cytotoxic activity *in vitro* (Table 2).

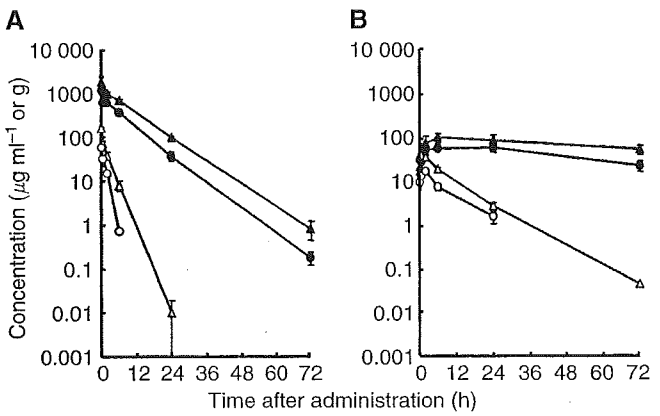


**Figure 2** Plasma and tumour concentrations of PTX after single i.v. administration of NK105 or PTX to Colon 26-bearing CDF1 mice. Plasma (**A**) and tumour (**B**) concentrations of PTX after NK105 administration at a PTX-equivalent dose of 50 $mg\,kg^{-1}$ (●), NK105 at a PTX-equivalent dose of 100 $mg\,kg^{-1}$ (▲), PTX 50 $mg\,kg^{-1}$ (○) and PTX 100 $mg\,kg^{-1}$ (△).

### *In vivo* antitumour activity

BALB/c mice bearing s.c. HT-29 colon cancer tumours showed decreased tumour growth rates after the administration of PTX and NK105. However, NK105 exhibited superior antitumour activity as compared with PTX ($P<0.001$). The antitumour activity of NK105 administered at a PTX-equivalent dose of 25 $mg\,kg^{-1}$ was comparable to that obtained after the administration of free PTX 100 $mg\,kg^{-1}$. Tumour suppression by NK105 increased in a dose-dependent manner. Tumours disappeared after the first dosing to mice treated with NK105 at a PTX-equivalent dose of 100 $mg\,kg^{-1}$, and all mice remained tumour-free thereafter (Figure 3A). In addition, less weight loss was induced in mice, which were given NK105 100 $mg\,kg^{-1}$ than in those that were given the same dose of free PTX (Figure 3B).

**Table 2** $IC_{50}$ values ($\mu M$) of PTX and NK105 in various cell lines

| | | 48 h | | 72 h | |
|---|---|---|---|---|---|
| **Cancer** | **Cell line** | **NK105** | **PTX** | **NK105** | **PTX** |
| Oesophageal cancer | TE-1 | > 1.0 | > 1.0 | 0.01 | 0.02 |
| | TE-8 | 0.02 | 0.02 | 0.01 | 0.01 |
| Lung cancer | PC-14 | 0.01 | 0.01 | 0.01 | 0.01 |
| | PC-14/TXT | 0.15 | 0.09 | 0.08 | 0.06 |
| | H460 | ND | ND | 0.03 | 0.01 |
| Breast cancer | MCF-7 | > 1.0 | > 1.0 | 0.01 | 0.01 |
| Stomach cancer | MKN-28 | 0.03 | 0.03 | 0.01 | 0.21 |
| | MKN-45 | 0.02 | 0.07 | 0.01 | 0.02 |
| Colon cancer | DLD-1 | 0.95 | 0.26 | 0.29 | 0.20 |
| | HT-29 | 0.01 | 0.01 | 0.01 | 0.01 |
| | HCT116 | ND | ND | 0.03 | 0.01 |
| Ovarian cancer | MCAS | 0.01 | 0.01 | 0.01 | 0.01 |
| | OVCAR-3 | > 1.0 | > 1.0 | > 1.0 | > 1.0 |
| Pancreatic cancer | AsPC-1 | ND | ND | 0.02 | 0.02 |
| | PAN-9 | ND | ND | 0.03 | 0.02 |
| | PAN-3 | ND | ND | 0.010 | 0.004 |

PTX = paclitaxel; ND = not done.

**Table 1** Pharmacokinetic parameters for the plasma and tumour concentrations of paclitaxel after single i.v. administration of NK105 and PTX to Colon 26-bearing CDF1 mice

| **Treatment** | **Dose ($mg\,kg^{-1}$)** | **$C_{5\,min}$ ($\mu g\,ml^{-1}$)** | **$t_{1/2}z$ (h)** | **$AUC_{0-t}$ ($\mu g\,h\,ml^{-1}$)** | **$AUC_{0-inf.}$ ($\mu g\,h\,ml^{-1}$)** | **$CL_{tot}$ ($ml\,h\,kg^{-1}$)** | **$V_{ss}$ ($ml\,kg^{-1}$)** |
|---|---|---|---|---|---|---|---|
| *Plasma* | | | | | | | |
| PTX | 50 | 59.32 | 0.98 | 90.2[a] | 91.3 | 547.6 | 684.6 |
| PTX | 100 | 157.67 | 1.84 | 309.0[b] | 309.0 | 323.6 | 812.2 |
| NK105 | 50 | 1157.03 | 5.99 | 7860.9[c] | 7862.3 | 6.4 | 46.4 |
| NK105 | 100 | 1812.37 | 6.82 | 15 565.7[c] | 15 573.6 | 6.4 | 54.8 |
| | | **$C_{max}$ ($\mu g\,ml^{-1}$)** | **$T_{max}$ (h)** | **$t_{1/2}z$ (h)** | **$AUC_{0-t}$ ($\mu g\,h\,ml^{-1}$)** | **$AUC_{0-inf.}$ ($\mu g\,h\,ml^{-1}$)** | |
| *Tumour* | | | | | | | |
| PTX | 50 | 12.50 | 2.0 | 7.02 | 120.8[b] | 133.0 | |
| PTX | 100 | 28.57 | 0.5 | 8.06 | 330.4[c] | 331.0 | |
| NK105 | 50 | 42.45 | 24.0 | 35.07 | 2360.1[c] | 3192.0 | |
| NK105 | 100 | 71.09 | 6.0 | 73.66 | 3884.9[c] | 7964.5 | |

i.v. = intravenous; $C_{5\,min}$ = plasma concentration at 5 min; $t_{1/2}z$ = half-life at the terminal phase; AUC = area under the curve; $CL_{tot}$ = total body clearance; $V_{ss}$ = volume of distribution at steady state; $T_{max}$ = time of maximum concentration; PTX = paclitaxel. Parameters were calculated from the mean value of three or two mice by noncompartmental analysis. [a]$AUC_{0-6h}$. [b]$AUC_{0-24h}$. [c]$AUC_{0-72h}$.

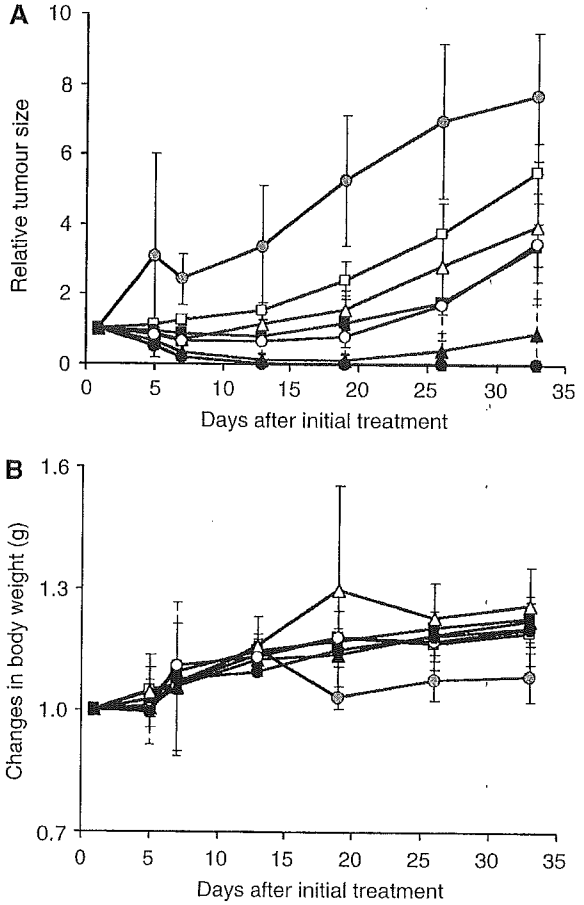


**Figure 3** Relative changes in HT-29 tumour growth rates in nude mice. (**A**) Effects of PTX (open symbols) and NK105 (closed symbols). PTX and NK105 were injected i.v. once weekly for 3 weeks at PTX-equivalent doses of 25 mg kg$^{-1}$ (□, ■), 50 mg kg$^{-1}$ (△, ▲), and 100 mg kg$^{-1}$ (○, ●), respectively. Saline was injected to control animals (●). (**B**) Changes in relative body weight. Data were derived from the same mice as those used for the present study.

### Neurotoxicity of PTX and NK105

Treatment with PTX has resulted in cumulative sensory-dominant peripheral neurotoxicity in humans, characterised clinically by numbness and/or paraesthesia of the extremities. Pathologically, axonal swelling, vesicular degeneration, and demyelination were observed. We, therefore, examined the effects of free PTX and NK105 using both electrophysiological and morphological methods.

Prior to drug administration, there were no significant differences in the amplitude of caudal sensory nerve action potential (caudal SNAP) between two drug administration groups. On day 6 after the last dosing (at week 6), the amplitude of the caudal SNAP in the control group increased in association with rat maturation. The amplitude was significantly smaller in the PTX group than in the control group ($P<0.01$), while the amplitude was significantly larger in the NK105 group than in the PTX group ($P<0.05$) and was comparable between the NK105 group and the control group (Figure 4A). Histopathological examination of longitudinal paraffin-embedded sections of the sciatic nerve 5 days after the sixth weekly injection revealed degenerative changes. The NK105 administration group showed only a few degenerative myelinated fibres in contrast to the PTX administration group, which indicated markedly more numerous degenerative myelinated fibres ($P<0.001$) (Figure 4B and C) and Table 3.

## DISCUSSION

A pharmacokinetic study revealed that the plasma AUC of NK105 was approximately 90-fold higher than that of free PTX in the present rodent models. Prolonged circulation of NK105 in the blood due to the EPR effect was associated with a significant increase in the tumour AUC. In fact, the tumour AUC of NK105 was approximately 25-fold higher than that of free PTX (Figure 2B). In mice, accordingly, NK105 exhibited stronger antitumour activity than free PTX (Figure 3A). However, it is still debatable whether or not the enhanced accumulation of an anticancer drug into a tumour is sufficient in leading the drug to exert its antitumour activity *in vivo*.

Jain *et al* have reported that the convective passage of large drug molecules into the core of solid tumours could be impeded by abnormally high interstitial pressures in solid tumours. However, they also admitted that low-molecular-weight anticancer agents might be harmful to normal organs because they can leak out of normal blood vessels freely; they finally concluded that one useful strategy for evading the barriers to drug dispersion would be to inject patients with drug carriers, such as liposomes, filled with low-molecular-weight drugs (Jain, 1994). In this case, liposomes should have sufficient time to exit from the site of tumour blood vessel leakage and to accumulate at reasonably high dose levels in the surrounding interstitium. Subsequently, low-molecular-weight drugs packed within liposomes should be released gradually so that they can be dispersed throughout the tumour. However, Unezaki *et al* have used fluorescence-labelled PEG-liposomes and described that the area of highest fluorescence was located outside tumour vessels, almost all around the vessel wall, even 2 days after drug injection (Unezaki *et al*, 1996). Therefore, the study suggested that although PEG-liposomes can be delivered effectively to a solid tumour via the EPR effect, the formulation would not be distributed sufficiently to cancer cells distant from tumour vessels because liposomes are too large to scamper about in the tumour interstitium. Liposomes have been suggested to be too stable to allow the drug therein to be released easily. Therefore, PEG-liposomes have been speculated to be not so effective against cancers in which the tumour vessel network is irregular and loose because of an abundant collagen-rich matrix. Such cancers include scirrhous cancer of the stomach and pancreatic cancer. In fact, Doxil®, a PEG-liposomal DXR, is known to be effective clinically against ovarian cancer and breast cancer, both of which are characterised by a high density of tumour microvessels; however, the drug is not effective against stomach cancer and pancreatic cancer (Muggia, 2001).

There are several possible reasons why NK105 exhibited higher antitumour activity in the present study as compared with free PTX: (1) since NK105 is very stable in the circulation and exhibits a markedly higher plasma AUC than free PTX, it accumulates better in tumour tissue than does free PTX due to the EPR effect; (2) NK105 is relatively small in size (85 nm) as compared with Doxil (100 nm), thus explaining its more uniform distribution in tumour tissue and its greater accumulation in cancer cells throughout cancer tissue. Savic *et al* (2003) have recently reported that polymeric micelles could internalise into cells to localise in several cytoplasmic organelles; and (3) a polymeric micelle carrier system for a drug has the potential to allow the effective sustained release of the drug inside a tumour following the accumulation of micelles into tumour tissue. Regarding NK105 in particular, this sustained release begins at a PTX-equivalent dose of $<1\,\mu g\,ml^{-1}$ (data not shown). Consequently, released PTX becomes distributed throughout tumour tissue and internalises into cancer cells to kill them.

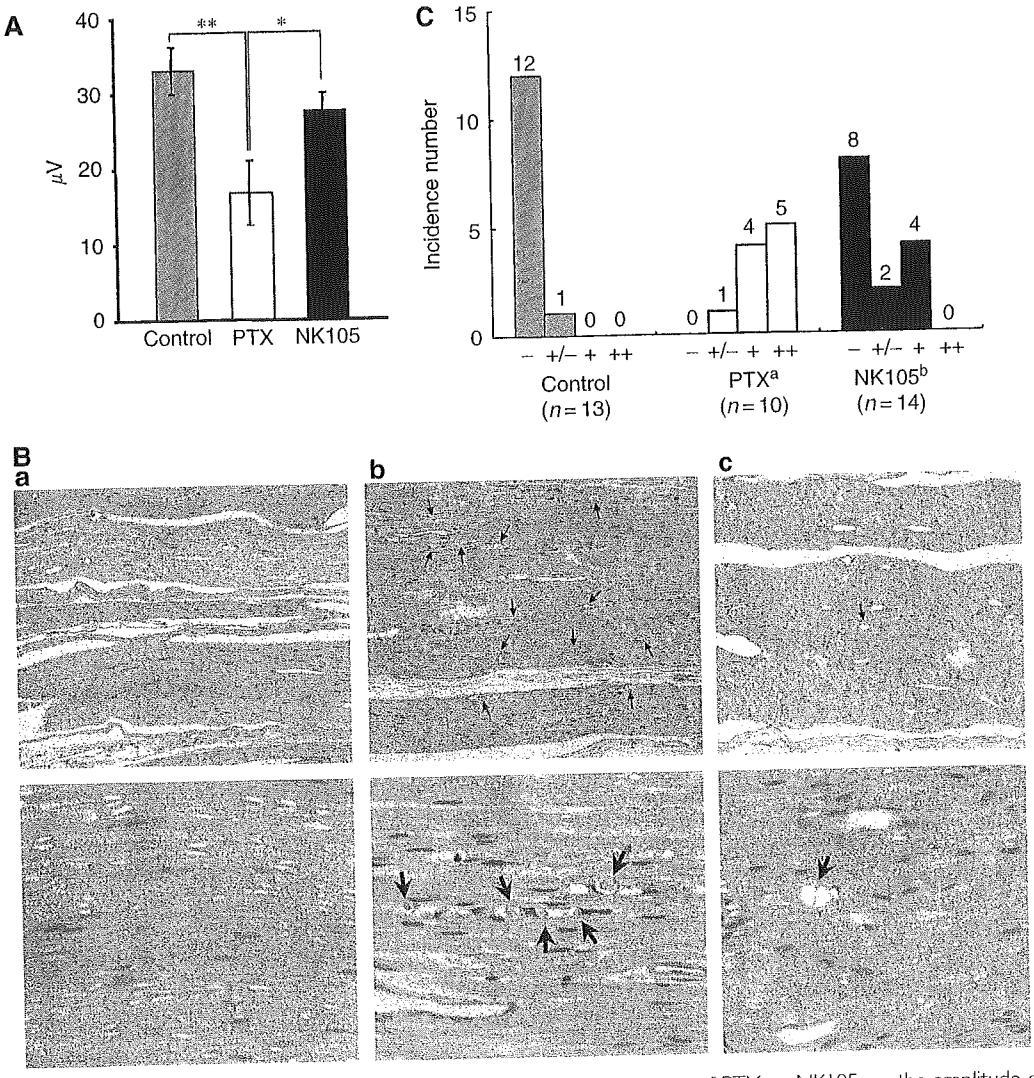


**Figure 4** Incorporation of PTX into polymeric micelles diminishes neurotoxicity. (**A**) Effects of PTX or NK105 on the amplitude of rat caudal sensory nerve action potentials as examined 5 days after weekly injections for 6 weeks. Rats ($n=14$) were injected with NK105 (■) or PTX (□) at a PTX-equivalent dose of 7.5 mg kg$^{-1}$. Glucose (5%) was also injected in the same manner to animals in the control group (■). $^{*}P<0.05$, $^{**}P<0.01$. (**B**) Histopathological changes in the sciatic nerve of rats. Degenerating myelinated nerve fibres (arrow) were examined in the longitudinal section of the sciatic nerve (H & E) 5 days after weekly injections for 6 weeks with 5% glucose (a), PTX (b), and NK105 (c) at a PTX-equivalent dose of 7.5 mg kg$^{-1}$. Magnification, × 100 (upper) and × 400 (lower). (**C**) Incidences of degenerating myelinated nerve fibres in rats treated with PTX or NK105. NK105 or PTX was administered i.v. at a weekly dose of 7.5 mg kg$^{-1}$ for 6 consecutive weeks to female rats. The degenerating myelinated fibre score was defined as follows: –, no degenerative changes; +/–, very slight degree of the degenerative changes (scattered, single fibres affected); +, slight degree of degenerative changes (scattered small groups of degenerative myelinated fibres); + +, moderate degree of degenerative changes (disseminated degenerative myelinated fibres); + + +, marked degree of degenerative changes (confluent groups of affected fibres). $^{a}P<0.001$ *vs* vehicle-treated animals. $^{b}P<0.001$ *vs* PTX-treated animals.

To date, PTX preparations that are categorised to DDSs have been developed. Among them, clinical trials are currently ongoing for the following drugs: CT-2103, polyglutamate-conjugated PTX (Singer *et al*, 2003); ABI-007, PTX coated with albumin (Ibrahim *et al*, 2002); and Genexol-PM, PTX micelle in which PTX is simply solubilised (Kim *et al*, 2004). The advantage commonly shared with these dosage forms is that they are injectable i.v. without the mixture of Cremophor EL and ethanol, which potentially provoke serious allergic reactions. The block copolymer used for forming NK105 micellar nanoparticles is nonimmunogenic and is injectable i.v. without Cremorphor EL and ethanol. Therefore, this dosage form is expected to possess a clinical advantage, which is similar to that of the above PTX dosage forms. Now, what is the difference between NK105 and other PTX dosage forms? ABI-007 and Genexol-PM were found to have the AUC and tumour AUC, which are nearly comparable or rather slightly lower than those of free PTX. Furthermore, the plasma AUC and tumour AUC are 11.5- and 11.8-fold higher, respectively, for CT-2103 than for free PTX, but they are markedly low as compared with those of NK105. Respective studies have employed proper tumours and proper rodent models. However, NK105 was forecasted to have markedly high plasma and tumour AUC as compared with those of other PTX dosage forms.

Regarding the toxicity profiles, the repeated administration of NK105 to rats at 7-day intervals produced less toxic effects on peripheral nerves than free PTX. This reduced the neurotoxicity of

**Table 3** Incidence of degenerating myelinated fibres in rats treated with PTX or NK105

| | | Degenerating myelinated nerve fibre score[b] | | | | |
|---|---|---|---|---|---|---|
| **Treatment** | ***n*[a]** | **–** | **+/–** | **+** | **++** | **+++** |
| Control (vehicle) | 13 | 12 | 1 | | | |
| PTX[c] | 10 | | 1 | 4 | 5 | |
| NK105[d] | 14 | 8 | 2 | 4 | | |

PTX = paclitaxel. Vehicle, NK105 or PTX was administered i.v. at a weekly dose of 7.5 mg kg$^{-1}$ for 6 consecutive weeks to female rats. [a]Total number of animals accounted for that experimental condition. [b]Degenerating myelinated fibre score was defined as follows: –, no degenerative changes; +/–, very slight degree of the degenerative changes (scattered, single fibres affected); +, slight degree of degenerative changes (scattered small groups of degenerative myelinated fibers); ++, moderate degree of degenerative changes (disseminated degenerative myelinated fibers); +++, marked degree of degenerative changes (confluent groups of affected fibres). [c]$P<0.001$ *vs* vehicle-treated animals. [d]$P<0.001$ *vs* PTX-treated animals.

NK105, which was demonstrated for the first time by both histopathological and physiological methods and was probably attributable to the less distribution of PTX into normal neural tissue following NK105 administration, since the volume of distribution at steady state ($V_{ss}$) of NK105 was 100-fold lower than that of free PTX. Regarding bone marrow toxicity, there was no difference between PTX and NK105 when 37.5 mg kg$^{-1}$ of PTX-equivalent dose was administered to rats weekly for 4 consecutive weeks (data not shown). These data indicate that NK105 warrants a clinical evaluation.

## ACKNOWLEDGEMENTS

We thank Dr H Uchino, Miss M Araake, and Mrs H Koike for their technical assistance. We are also grateful to Mrs K Shiina and Miss H Orita for their secretarial assistance. This work was supported by a Grant-in-Aid from the Ministry of Health, Labor and Welfare of Japan (Y Matsumura).

## REFERENCES

Carney DN (1996) Chemotherapy in the management of patients with inoperable non-small cell lung cancer. *Semin Oncol* **23:** 71–75

Hamaguchi T, Matsumura Y, Shirao Y, Shimada Y, Yamada Y, Muro Y, Okusaka T, Ueno H, Ikeda M, Watanabe N (2003) Phase I study of novel drug delivery system, NK911, a polymer micelle encapsulated doxorubicin. *Proc Am Soc Clin Oncol* **22:** 571

Ibrahim NK, Desai N, Legha S, Soon-Shiong P, Theriault RL, Rivera E, Esmaeli B, Ring SE, Bedikian A, Hortobagyi GN, Ellerhorst JA (2002) Phase I and pharmacokinetic study of ABI-007, a Cremophor-free, protein-stabilized, nanoparticle formulation of paclitaxel. *Clin Cancer Res* **8:** 1038–1044

Jain RK (1994) Barriers to drug delivery in solid tumours. *Sci Am* **271:** 58–65

Kataoka K, Kwon GS, Yokoyama M, Okano T, Sakurai Y (1993) Block copolymer micelles as vehicles for drug delivery. *J Control Rel* **24:** 119–132

Khayat D, Antoine EC, Coeffic D (2000) Taxol in the management of cancers of the breast and the ovary. *Cancer Invest* **18:** 242–260

Kim TY, Kim DW, Chung JY, Shin SG, Kim SC, Heo DS, Kim NK, Bang YJ (2004) Phase I and pharmacokinetic study of Genexol-PM, a cremophor-free, polymeric micelle-formulated paclitaxel, in patients with advanced malignancies. *Clin Cancer Res* **10:** 3708–3716

Kwon GS, Suwa S, Yokoyama M, Okano T, Sakurai Y (1994) Enhanced tumour accumulation and prolonged circulation times of micelle-forming poly(ethylene oxide-aspartic) block copolymer–adriamycin conjugate. *J Control Rel* **29:** 17–23

Maeda H, Wu J, Sawa T, Matsumura Y, Hori K (2000) Tumour vascular permeability and the EPR effect in macromolecular therapeutics: a review. *J Control Rel* **65:** 271–284

Matsumura Y, Maeda H (1986) A new concept for macromolecular therapeutics in cancer chemotherapy: mechanism of tumouritropic accumulation of proteins and the antitumour agent smancs. *Cancer Res* **46:** 6387–6392

Muggia FM (2001) Liposomal encapsulated anthracyclines: new therapeutic horizons. *Curr Oncol Rep* **3:** 156–162

Nakanishi T, Fukushima S, Okamoto K, Suzuki M, Matsumura Y, Yokoyama M, Okano T, Sakurai Y, Kataoka K (2001) Development of the polymer micelle carrier system for doxorubicin. *J Control Rel* **74:** 295–302

Rowinsky EK, Chaudhry V, Forastiere AA, Sartorius SE, Ettinger DS, Grochow LB, Lubejko BG, Cornblath DR, Donehower RC (1993) Phase I and pharmacologic study of paclitaxel and cisplatin with granulocyte colony-stimulating factor: neuromuscular toxicity is dose-limiting. *J Clin Oncol* **11:** 2010–2020

Rowinsky EK, Donehower RC (1995) Paclitaxel (taxol). *N Engl J Med* **332:** 1004–1014

Savic R, Luo L, Eisenberg A, Maysinger D (2003) Micellar nanocontainers distribute to defined cytoplasmic organelles. *Science* **300:** 615–618

Singer JW, Baker B, De Vries P, Kumar A, Shaffer S, Vawter E, Bolton M, Garzone P (2003) Poly-(L)-glutamic acid-paclitaxel (CT-2103) [XYOTAX], a biodegradable polymeric drug conjugate: characterization, preclinical pharmacology, and preliminary clinical data. *Adv Exp Med Biol* **519:** 81–99

Unezaki S, Maruyama K, Hosoda J, Nagai I, Koyanagi Y, Nakata M, Ishida O, Iwatsuru M, Tsuchiya S (1996) Direct measurement of the extravasation of polyethylene glycol-coated liposomes into solid tumour tissue by *in vivo* fluorescence microscopy. *Int J Pharmacol* **144:** 11–17

Wasserheit C, Frazein A, Oratz R, Sorich J, Downey A, Hochster H, Chachoua A, Wernz J, Zeleniuch-Jacquotte A, Blum R, Speyer J (1996) Phase II trial of paclitaxel and cisplatin in women with advanced breast cancer: an active regimen with limiting neurotoxicity. *J Clin Oncol* **14:** 1993–1999

Weiss RB, Donehower RC, Wiernik PH, Ohnuma T, Gralla RJ, Trump DL, Baker Jr JR, Van Echo DA, Von Hoff DD, Leyland-Jones B (1990) Hypersensitivity reactions from taxol. *J Clin Oncol* **8:** 1263–1268

Yokoyama M, Miyauchi M, Yamada N, Okano T, Sakurai Y, Kataoka K, Inoue S (1990) Polymer micelles as novel drug carrier:adriamycin-conjugated poly(ethylene glycol)-poly(aspartic acid) block copolymer. *J Control Rel* **11:** 269–278

Yokoyama M, Okano T, Sakurai Y, Ekimoto H, Shibazaki C, Kataoka K (1991) Toxicity and antitumour activity against solid tumours of micelle-forming polymeric anticancer drug and its extremely long circulation in blood. *Cancer Res* **51:** 3229–3236

Yokoyama M, Okano T, Sakurai Y, Fukushima S, Okamoto K, Kataoka K (1999) Selective delivery of adriamycin to a solid tumour using a polymeric micelle carrier system. *J Drug Target* **7:** 171–186

0022-5347/05/1735-1767/0
THE JOURNAL OF UROLOGY®

Vol. 173, 1767–1771, May 2005
*Printed in U.S.A.*
**DOI: 10.1097/01.ju.0000154632.11824.4d**

# DNA HYPERMETHYLATION ON MULTIPLE CpG ISLANDS ASSOCIATED WITH INCREASED DNA METHYLTRANSFERASE DNMT1 PROTEIN EXPRESSION DURING MULTISTAGE UROTHELIAL CARCINOGENESIS

TOHRU NAKAGAWA, YAE KANAI,* SAORI USHIJIMA, TADAICHI KITAMURA, TADAO KAKIZOE AND SETSUO HIROHASHI

*From the Pathology Division, National Cancer Center Research Institute (TN, YK, SU, SH), Department of Urology, Faculty of Medicine, Tokyo University (TN, TKi) and National Cancer Center (TKa), Tokyo Japan*

ABSTRACT

Purpose: We elucidated the significance of aberrant DNA methylation on multiple CpG islands and its correlation with DNA methyltransferase DNMT1 protein expression during urothelial carcinogenesis.

Materials and Methods: We examined the DNA methylation status on multiple CpG islands by methylation specific polymerase chain reaction and combined bisulfite restriction enzyme analysis in 12 specimens of normal urothelium, 23 of noncancerous urothelium showing no remarkable histological changes obtained from patients with bladder cancer (NBC) and 70 of transitional cell carcinoma (TCC).

Results: DNA methylation on CpG islands of the *p16* (0%, 17% and 21%) and *death-associated protein kinase* (13%, 33% and 29%) genes, and methylated in tumor-2 (56%, 60% and 76%), 12 (0%, 6% and 30%), 25 (25%, 27% and 35%) and 31 (45%, 56% and 79%) clones was detected in normal urothelium, NBCs and TCCs, respectively. The incidence of concurrent DNA hypermethylation on 3 or more CpG islands in NBCs (38%) was significantly higher than that in normal urothelium (0%, $p = 0.0455$) and even higher in TCCs (59%, $p = 0.0043$). The incidence of the CpG island methylator phenotype in nonpapillary carcinomas (nodular invasive carcinomas and their precursors, ie flat carcinoma in situ, 71%) was significantly higher than in papillary carcinomas (40%, $p = 0.0143$). In all specimens examined concurrent DNA hypermethylation on 3 or more CpG islands significantly correlated with immunohistochemically evaluated DNMT1 protein over expression ($p = 0.0167$).

Conclusions: DNA hypermethylation on multiple CpG islands in association with DNMT1 protein over expression may participate in multistage urothelial carcinogenesis even at the precancerous stage and particularly in the development of nodular invasive carcinomas of the bladder.

KEY WORDS: carcinoma, transitional cell; bladder; CpG islands; phenotype; DNA

DNA methylation has important roles in transcriptional regulation, chromatin remodeling and genomic stability. Overall DNA hypomethylation accompanied by region specific hypermethylation is generally observed in human cancers.[1] Aberrant DNA methylation may have roles in carcinogenesis as a result of 1) increased gene mutagenicity due to the deamination of 5-methylcytosine to thymine, 2) the possible association of aberrant DNA methylation with allelic loss and 3) the repression of gene transcription through the methylation of CpG islands in regulatory regions of specific genes, including tumor suppressor genes.[1] In transitional cell carcinomas (TCCs) of the bladder hypermethylation on CpG islands around the promoter region and decreased expression of tumor suppressor genes, such as the *p16* and *E-cadherin* genes, have been reported.[2,3] Regional DNA hypermethylation correlates significantly with poor prognosis in patients with TCC.[2] However, only a limited number of groups have examined aberrant DNA methylation with regard to precancerous conditions and the histological heterogeneity of TCCs.

Increased mRNA and protein expression of DNA methyltransferase DNMT1 is reported to correlate significantly with the CpG island methylator phenotype (CIMP), defined as frequent DNA hypermethylation on CpG islands that are not normally methylated,[4] in colorectal and stomach cancers.[5,6] We have previously reported that DNMT1 protein expression is already increased in noncancerous urothelium showing no remarkable histological changes obtained from patients with bladder cancer (NBC), preceding the increase in cell proliferative activity reflected by the proliferating cell nuclear antigen (PCNA) labeling index.[7] Such urothelium can be considered precancerous because it may be exposed to carcinogens in the urine. Progressively increasing expression of DNMT1 protein is particularly associated with the development of flat carcinoma in situ (CIS), which is considered to be a precursor of nodular invasive carcinoma of the bladder.[7] However, to our knowledge no studies have determined whether in fact DNMT1 over expression results in DNA hypermethylation on CpG islands during urothelial carcinogenesis.

To determine the significance of aberrant DNA methylation and examine whether increased DNMT1 protein expression is the underlying mechanism for this aberrant

Submitted for publication August 5, 2004.
Supported by a Grant-in-Aid for the Second Term Comprehensive 10-Year Strategy for Cancer Control and a Grant-in-Aid for Cancer Research, Ministry of Health, Labor and Welfare of Japan, and a Research Resident Fellowship from the Foundation for Promotion of Cancer Research in Japan (TN).
* Correspondence: Pathology Division, National Cancer Center Research Institute, 5–1-1 Tsukiji, Chuo-ku, Tokyo 104-0045, Japan (FAX: 81–3-3248–2463; e-mail: ykanai@ncc.go.jp).

methylation during human urothelial carcinogenesis we examined DNA methylation status on multiple CpG islands in normal urothelium, NBCs and TCCs. We also examined the correlation between DNA methylation status and immunohistochemically evaluated DNMT1 protein expression.

## MATERIALS AND METHODS

*Patients and tissue samples.* A total of 23 specimens of NBC and 70 of TCC were obtained from surgically resected specimens of patients who underwent radical cystectomy (40) or transurethral resection of bladder tumor (15) at National Cancer Center Hospital, Tokyo, Japan. The study group comprised 44 men and 11 women with a mean age ± SD of 62.4 ± 11.9 years (range 39 to 89). The 70 TCC specimens were classified histologically as pTa in 29, pTis in 14, pT1 in 7 and pT2 to pT3 in 20 according to criteria proposed by the International Union Against Cancer.[8] That is, there were 29 papillary (noninvasive, pTa) tumors and 41 nonpapillary tumors (flat CIS or pTis and invasive carcinoma, pT1 to pT3). For comparison, 12 specimens of normal urothelium were also obtained from specimens surgically resected from 12 patients who underwent total pelvic exenteration for primary or locally recurrent rectal cancers. This patient group comprised 9 men and 3 women with a mean age of 56.1 ± 9.0 years (range 37 to 70). For 89 of these 105 specimens we have previously reported the results of immunohistochemical examination for DNMT1.[7]

*Methylation specific polymerase chain reaction (PCR) (MSP) and combined bisulfite restriction enzyme analysis (COBRA).* Sections (10 μm) from formalin fixed, paraffin embedded specimens were mounted on microscope slides, deparaffinized and stained with hematoxylin and eosin. Cancerous and noncancerous urothelium was collected under a stereoscopic microscope using a fine needle, avoiding potential contamination between each cell type or with stromal and inflammatory cells (fig. 1). DNA was isolated from microdissected specimens by a standard procedure involving proteinase-K treatment, phenol-chloroform extraction and ethanol precipitation.

Bisulfite conversion of DNA was done with a CpGenome DNA Modification Kit (Intergen, Purchase, New York) in accordance with manufacturer instructions. DNA methylation status on CpG islands of the *p16* gene was determined by MSP[9] using primer sets provided in a CpG WIZ amplification kit (Intergen). DNA methylation status on the *death-associated protein kinase* (*DAPK*) gene, and on methylated in tumor (MINT)-2, 12, 25 and 31 clones was determined by COBRA.[10] Bisulfite modified DNA was amplified by PCR using previously described primers[4,11] and digested with restriction enzymes, including BstUI for the *DAPK* gene, and MINT-2 and 31 clones, MaeII for the MINT-12 clone and RsaI for the MINT-25 clone. Reaction products were separated electrophoretically on 3% agarose gel and stained with ethidium bromide. Signal intensity was measured with an image analyzer (Model FMBIO-2, Takara, Ohtsu, Japan).

*Statistics.* Correlations between the incidence of concurrent DNA hypermethylation on 3 or more CpG islands or CIMP on 1 hand, and clinicopathological parameters or DNMT1 immunoreactivity on the other hand were analyzed by the chi-square test with $p < 0.05$ considered significant.

## RESULTS

*DNA methylation status on multiple CpG islands in noncancerous urothelium and TCCs.* Figure 2 shows examples of PCR products from MSP and COBRA. DNA methylation on CpG islands of the *p16* gene was detected in 0 of the 9 examined normal urothelium samples (0%), in 3 of the 18 examined NBCs (17%) and in 13 of the 62 examined TCCs (21%). DNA methylation of the *DAPK* gene was detected in 1 of the 8 normal urothelium samples (13%), in 6 of the 18 NBCs (33%) and in 18 of the 63 TCCs (29%). DNA methylation of the MINT-2 clone was detected in 5 of the 9 normal urothelium samples (56%), in 13 of the 22 NBCs (60%) and in 52 of the 68 TCCs (76%). DNA methylation of the MINT-12 clone was detected in 0 of the 8 normal urothelium samples (0%), in 1 of the 18 NBCs (6%) and in 20 of the 67 TCCs (30%). DNA methylation of the MINT-25 clone was detected in 2 of the 8 normal urothelium samples (25%), in 4 of the 15 NBCs (27%) and in 22 of the 62 TCCs (35%). DNA methylation of the MINT-31 clone was detected in 5 of the 11 normal urothelium samples (45%), in 10 of the 18 NBCs (56%) and in 52 of the 66 TCCs (79%). Although DNA methylation on some CpG islands was detected even in normal urothelium, the incidence in normal urothelium did not correlate with patient age (data not shown). Generally the incidence of DNA methylation on each CpG island increased progressively from normal urothelium to NBCs and then to TCCs.

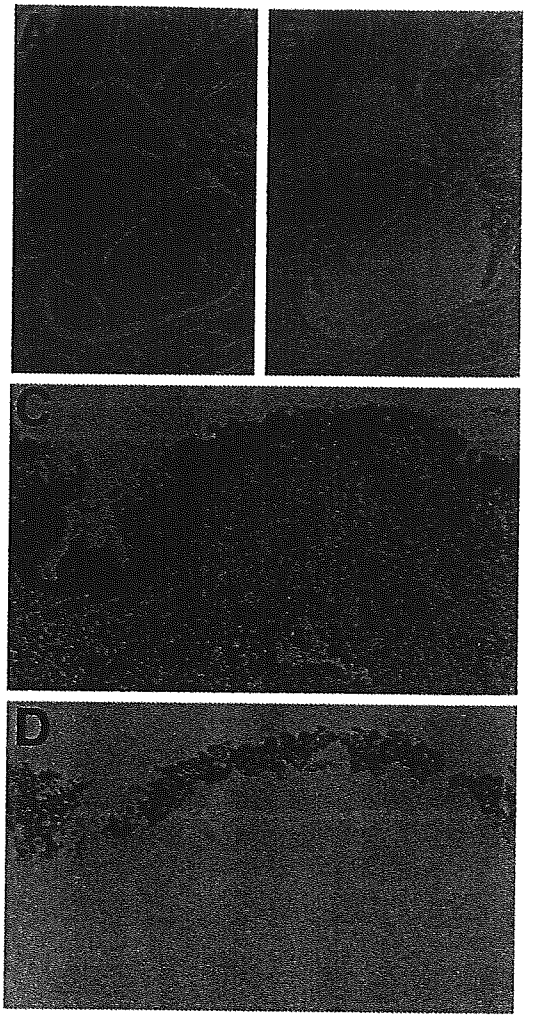


FIG. 1. Representative specimens of TCC, including specimen T18 of nodular invasive carcinoma (*A* and *B*) and specimen T31 of CIS (*C* and *D*) before (*A* and *C*), during (*D*) and after (*B*) microdissection. Single asterisks indicate invasive carcinoma specimen (*A*) collected without contamination with stromal and inflammatory cells (*B*). Double asterisks indicate subepithelial tissue (*C*) removed to avoid contamination (*D*) before collecting flat CIS specimens. Reduced from ×50 (*A* and *B*) and ×90 (*C* and *D*)

Previously described criteria have defined cancers showing DNA hypermethylation on 3 or more CpG islands that are not methylated in an age dependent manner as CIMP positive when 5 or more of such CpG islands are examined.[4] Figure 3 shows DNA methylation status on each CpG island in 87 specimens of normal urothelium, NBC and TCC, in

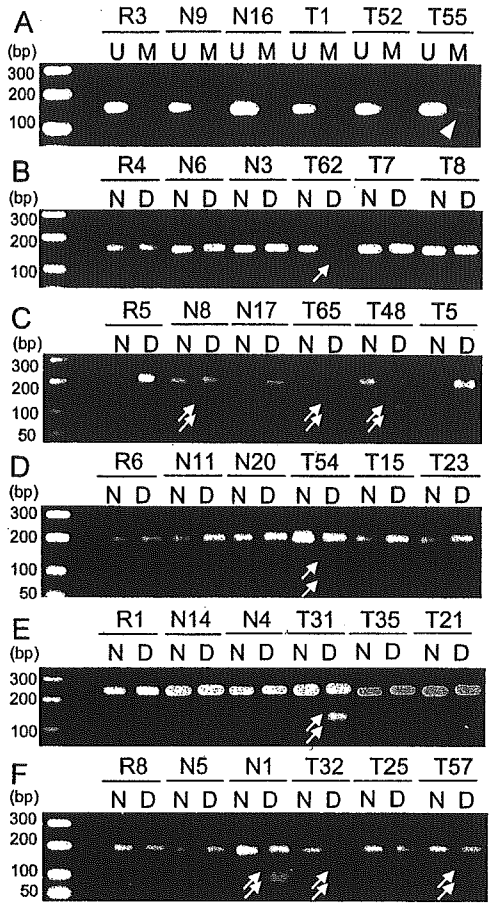


FIG. 2. Examples of PCR products from DNA methylation analyses of multiple CpG islands in patients with or without bladder cancer. DNA methylation status on CpG islands of *p16* gene (*A*) was evaluated by MSP. In this analysis PCR products generated by primer sets reflected presence of methylated (*M*, arrowhead) and unmethylated (*U*) genes. DNA methylation on CpG islands of *DAPK* (*B*) gene, and MINT-2, 12, 25 and 31 clones (*C* to *F*, respectively) was evaluated by COBRA. In this analysis only methylated genes (arrows) were digested by restriction enzymes. *R*, normal urothelium obtained from patients who underwent total pelvic exenteration for rectal cancer. *N*, noncancerous urothelium showing no remarkable histological changes obtained from patients with bladder cancer. *T*, TCC. *N*, non-digestion with restriction enzyme. *D*, digestion with restriction enzyme.

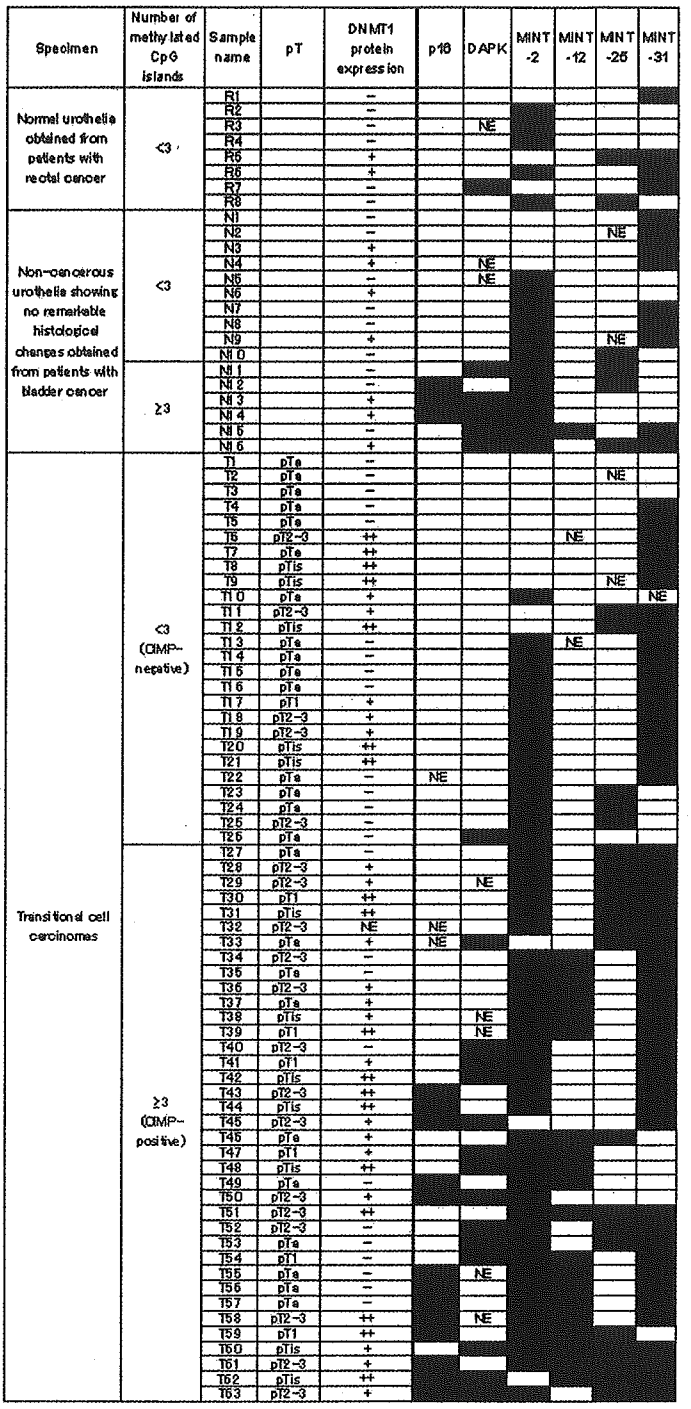


FIG. 3. DNA methylation profiles for CpG islands and protein expression levels of DNMT1 in specimens in which 5 or all 6 CpG islands could be evaluated. DNA methylation status was examined by MSP or COBRA (fig. 2). DNMT1 protein expression levels were defined as described. Vertical columns indicate specimen number, invasion depth in TCC specimens and protein expression of DNMT1. Top row indicates CpG islands. Filled box indicates methylated. Open box indicates unmethylated. *NE*, not evaluable.

which 5 or all 6 CpG islands could be evaluated. However, we examined DNA methylation status on only 4 or fewer CpG islands in the remaining 18 specimens because of a shortage of DNA extracted from the microdissected samples. Concurrent DNA methylation on 3 or more CpG islands was detected in 0 of the 8 normal urothelium samples (0%), 6 of the 16 NBCs (38%) and 37 of the 63 TCCs (59%). Such TCCs were considered CIMP positive based on described criteria.[4] The incidence of concurrent DNA hypermethylation on 3 or more CpG islands increased progressively from normal urothelium to NBCs and then to TCCs (chi-square test $p = 0.0043$). Even in NBCs it was significantly higher than in normal urothelium (chi-square test $p = 0.0455$).

*Correlation between DNA methylation status on multiple CpG islands and clinicopathological parameters in TCC 23 (52%).* Of the 44 specimens of superficial carcinoma (pTa, pTis and pT1) and 14 (74%) of 19 of invasive carcinoma (pT2 to pT4) were CIMP positive. Invasion depth (pTa, pTis and pT1 vs pT2 to pT4) did not significantly correlate with CIMP (chi-square test $p = 0.1131$). Ten of 25 specimens (40%) of papillary carcinoma (pTa) and 27 of 38 (71%) of nonpapillary carcinoma (flat CIS or pTis and invasive carcinoma pT1 or greater) were CIMP positive. The incidence of CIMP was significantly higher in nonpapillary than in papillary carcinomas (chi-square test $p = 0.0143$). Among nonpapillary carcinomas there was no significant difference in the incidence of CIMP between flat CIS (pTis in 7 or 12 specimens or 58%) and invasive carcinomas (pT1 or greater in 20 of 26 or 77%) (chi-square test $p = 0.2402$).

*Correlation between DNA methylation status on multiple CpG islands and DNMT1 protein expression during multistage urothelial carcinogenesis.* We have previously reported

the results of immunohistochemical examination for DNMT1 in 89 of the current 105 specimens.[7] We subjected the remaining 16 specimens to the same immunohistochemical examination for DNMT1. DNMT1 immunoreactivity of a tissue sample was considered positive (+) if more than 30% of cells showed the same nuclear staining intensity as positive internal control lymphocytes, and strongly positive (++) if more than 30% of cells showed stronger intensity, as described previously.[7] Figure 3 shows the intensity of DNMT1 immunoreactivity in the 86 specimens for which DNA methylation status on 5 or all 6 CpG islands could be evaluated. In 86 specimens of normal urothelium, NBC and TCC concurrent DNA hypermethylation on 3 or more CpG islands significantly correlated with increased (+ or ++) DNMT1 protein expression (chi-square test $p = 0.0167$).

## DISCUSSION

The incidence of aberrant DNA hypermethylation, such as concurrent DNA methylation on 3 or more CpG islands, was significantly higher in NBCs than in normal urothelium. TCCs are notorious for their clinical features of multicentricity and tendency toward recurrence. Synchronously or metachronously multifocal TCCs often develop in certain patients. Although multifocal development of TCCs may be partly attributable to intraluminal seeding, a possible mechanism for multiplicity is the field effect, whereby carcinogenic agents in urine cause malignant transformation of multiple urothelial cells.[12] Even noncancerous urothelium showing no remarkable histological changes can be considered precancerous, because they may be exposed to carcinogens in the urine. Our data suggest that aberrant DNA hypermethylation on multiple CpG islands may participate even in precancerous conditions during multistage urothelial carcinogenesis.

CIMP did not correlate with TCC aggressiveness (eg depth of invasion) but it significantly correlated with morphological structure (papillary vs nonpapillary). Bladder carcinomas are classified as papillary or nodular according to their macroscopic configurations. Papillary carcinomas usually remain noninvasive, although patients must undergo repeat cystoscopic resection because of recurrences.[13] In contrast, the clinical outcome of nodular invasive carcinomas is poor.[13] Flat CIS, which frequently spreads widely and is sometimes scattered over the bladder, is associated with nodular invasive carcinomas. Frequent *p53* gene mutations[14] and loss of heterozygosity on chromosome 14q[15] indicated a common background for flat CIS and invasive carcinomas and, therefore, flat CIS is considered a precursor of nodular invasive carcinomas of the bladder. In this study we successfully examined DNA methylation status even in flat CIS, which was macroscopically indistinguishable from noncancerous urothelium, using microdissection techniques. Our results suggest that CIMP is particularly associated with the development of flat CIS and nodular invasive carcinomas with a poorer prognosis.

DNMT1 targets replication foci, where DNA methylation patterns are copied from the mother strand, by binding to PCNA.[16] However, excessive amounts of DNMT1, which cannot target replication foci, may participate in de novo methylation of CpG islands that are not methylated in normal cells. In addition, targeting of substrate DNA by DNMT1 may be disrupted by mechanisms, such as dysfunction of p21WAF1,[17] which competes with DNMT1 for binding to PCNA, in cancer cells.[16] Moreover, it was recently suggested that DNMT1 is capable of de novo methylating activity as well as having a maintenance function.[18,19] Therefore, it is feasible that in cancers DNMT1 participates in regional DNA hypermethylation on CpG islands. The incidence of concurrent DNA hypermethylation on 3 or more CpG islands significantly correlated with increased DNMT1 protein expression in all examined specimens of normal urothelium, NBC and TCC, suggesting the possibility that the previously proven DNMT1 over expression actually resulted in frequent regional DNA hypermethylation during urothelial carcinogenesis.

DNMT1 mRNA is expressed mainly during the S-phase.[1] Because tumor tissue presumably contains a greater proportion of dividing cells than normal tissue does, it has been debatable whether increased DNMT1 expression is due to an increase in the proportion of dividing cells or to an acute increase in DNMT1 expression per individual cell.[20] However, we have previously reported that DNMT1 expression levels are already increased in NBCs in which the PCNA labeling index has not yet increased.[7] Increased DNMT1 expression did not result entirely from increased numbers of dividing cells in the tissues examined, but rather it clearly preceded increased cell division.[7] In our current study the incidence of concurrent DNA methylation on 3 or more CpG islands was significantly higher in NBCs than in normal urothelium, in parallel with the previously proven DNMT1 over expression. Moreover, the frequent regional DNA hypermethylation observed in our current study and the previously proven DNMT1 over expression were associated with the pathway of development of CIS and nodular invasive carcinomas. These data further support the concept that the previously proven DNMT1 over expression resulted in frequent regional DNA hypermethylation during urothelial carcinogenesis.

In our previous study in nonpapillary carcinomas DNMT1 protein expression was significantly higher in flat CIS than in invasive carcinomas.[7] On the other hand, in our current study there was no difference in the incidence of CIMP between flat CIS and invasive carcinomas. After markedly over expressed DNMT1 induces de novo DNA hypermethylation on multiple CpG islands at the stage of flat CIS, aberrant DNA methylation status may be maintained successfully even if DNMT1 expression is decreased to some extent in invasive carcinomas.

Although DNMT1 is a major DNA methyltransferase in humans, to date 2 other enzymes, namely DNMT3a and DNMT3b, have also been shown to possess DNA methyltransferase activity.[1] Genomic methylation patterns may be established through cooperation among these 3 enzymes even in cancer cells.[19] Further studies of how cooperation between DNMT1 and other components of the DNA methylation machinery affects DNA methylation status in tissue specimens may increase our understanding of the basis of regional DNA hypermethylation during urothelial carcinogenesis.

## REFERENCES

1. Jones, P. A. and Baylin, S. B.: The fundamental role of epigenetic events in cancer. Nat Rev Genet, **3:** 415, 2002
2. Maruyama, R., Toyooka, S., Toyooka, K. O., Harada, K., Virmani, A. K., Zochbauer-Muller, S. et al: Aberrant promoter methylation profile of bladder cancer and its relationship to clinicopathological features. Cancer Res, **61:** 8659, 2001
3. Horikawa, Y., Sugano, K., Shigyo, M., Yamamoto, H., Nakazono, M., Fujimoto, H. et al: Hypermethylation of an E-cadherin (CDH1) promoter region in high grade transitional cell carcinoma of the bladder comprising carcinoma in situ. J Urol, **169:** 1541, 2003
4. Toyota, M., Ahuja, N., Ohe-Toyota, M., Herman, J. G., Baylin, S. B. and Issa, J. P.: CpG island methylator phenotype in colorectal cancer. Proc Natl Acad Sci USA, **96:** 8681, 1999
5. Kanai, Y., Ushijima, S., Kondo, Y., Nakanishi, Y. and Hirohashi, S.: DNA methyltransferase expression and DNA methylation of CpG islands and peri-centromeric satellite regions in human colorectal and stomach cancers. Int J Cancer, **91:** 205, 2001
6. Etoh, T., Kanai, Y., Ushijima, S., Nakagawa, T., Nakanishi, Y., Sasako, M. et al: Increased DNA methyltransferase 1

(DNMT1) protein expression correlates significantly with poorer tumor differentiation and frequent DNA hypermethylation of multiple CpG islands in gastric cancers. Am J Pathol, **164:** 689, 2004
7. Nakagawa, T., Kanai, Y., Saito, Y., Kitamura, T., Kakizoe, T. and Hirohashi, S.: Increased DNA methyltransferase 1 protein expression in human transitional cell carcinoma of the bladder. J Urol, **170:** 2463, 2003
8. Sobin, L. H. and Wittekind, C. H.: TNM Classification of Malignant Tumors, 5th ed. New York: Wiley-Liss, Inc., 1997
9. Herman, J. G., Graff, J. R., Myohanen, S., Nelkin, B. D. and Baylin, S. B.: Methylation-specific PCR: a novel PCR assay for methylation status of CpG islands. Proc Natl Acad Sci USA, **93:** 9821, 1996
10. Xiong, Z. and Laird, P. W.: COBRA: a sensitive and quantitative DNA methylation assay. Nucleic Acids Res, **25:** 2532, 1997
11. Satoh, A., Toyota, M., Itoh, F., Kikuchi, T., Obata, T., Sasaki, Y. et al: DNA methylation and histone deacetylation associated with silencing DAP kinase gene expression in colorectal and gastric cancers. Br J Cancer, **86:** 1817, 2002
12. Harris, A. L. and Neal, D. E.: Bladder cancer—field versus clonal origin. N Engl J Med, **326:** 759, 1992
13. Friedell, G. H., Parija, G. C., Nagy, G. K. and Soto, E. A.: The pathology of human bladder cancer. Cancer, **45:** 1823, 1980
14. Spruck, C. H., 3rd, Ohneseit, P. F., Gonzalez-Zulueta, M., Esrig, D., Miyao, N., Tsai, Y. C. et al: Two molecular pathways to transitional cell carcinoma of the bladder. Cancer Res, **54:** 784, 1994
15. Chang, W. Y., Cairns, P., Schoenberg, M. P., Polascik, T. J. and Sidransky, D.: Novel suppressor loci on chromosome 14q in primary bladder cancer. Cancer Res, **55:** 3246, 1995
16. Chuang, L. S., Ian, H. I., Koh, T.W., Ng, H. H., Xu, G. and Li, B. F.: Human DNA-(cytosine-5) methyltransferase-PCNA complex as a target for p21WAF1. Science, **277:** 1996, 1997
17. Baylin, S. B.: Tying it all together: epigenetics, genetics, cell cycle and cancer. Science, **277:** 1948, 1997
18. Vertino, P. M., Yen, R. W., Gao, J. and Baylin, S. B.: De novo methylation of CpG island sequences in human fibroblasts overexpressing DNA (cytosine-5-)-methyltransferase. Mol Cell Biol, **16:** 4555, 1996
19. Rhee, I., Bachman, K. E., Park, B. H., Jair, K. W., Yen, R. W., Schuebel, K. E. et al: DNMT1 and DNMT3b cooperate to silence genes in human cancer cells. Nature, **416:** 552, 2002
20. Lee, P. J., Washer, L. L., Law, D. J., Boland, C. R., Horon, I. L. and Feinberg, A. P.: Limited up-regulation of DNA methyltransferase in human colon cancer reflecting increased cell proliferation. Proc Natl Acad Sci USA, **93:** 10366, 1996

Laboratory Investigation (2005) 85, 895–907

www.laboratoryinvestigation.org

# Loss of blood group A antigen expression in bladder cancer caused by allelic loss and/or methylation of the *ABO* gene

Yoshitomo Chihara[1,2], Kokichi Sugano[1], Ayumi Kobayashi[1], Yae Kanai[3], Hidenobu Yamamoto[4], Masaaki Nakazono[4], Hiroyuki Fujimoto[5], Tadao Kakizoe[5], Kiyohide Fujimoto[2], Setsuo Hirohashi[4] and Yoshihiko Hirao[2]

[1]*Oncogene Research Unit/Cancer Prevention Unit, Tochigi Cancer Center Research Institute, Tochigi, Japan;* [2]*Department of Urology, Nara Medical University, Nara, Japan;* [3]*Pathology Division, National Cancer Center Research Institute, Tokyo, Japan;* [4]*Department of Urology, Tochigi Cancer Center Hospital, Tochigi, Japan and* [5]*Department of Urology, National Cancer Center Hospital, Tokyo, Japan*

**Loss of ABO blood group antigen expression has been reported in transitional cell carcinoma (TCC) of the bladder. Synthesis of the ABO blood group antigen was genetically determined by allelic variants of the *ABO* gene assigned on 9q34.1. We analyzed loss of heterozygosity (LOH) and promoter hypermethylation of the *ABO* gene in TCC and compared them with alterations of A antigen expression in TCC, dysplasia and normal urothelium. A total of 81 samples of TCC of the bladder obtained from transurethral resection (TUR) ($n=44$) and radical cystectomy ($n=37$) were examined. Expression of the A antigen was evaluated by immunohistochemical staining (IHC) using anti-A antigen monoclonal antibody. LOH of the *ABO* gene locus was examined by blunt-end single-strand DNA conformational polymorphism (SSCP) analysis using flouresence-based auto sequencer. Promoter hypermethylation of the *ABO* gene were examined by bisulfite PCR-SSCP (BiPS) analysis and/or methylation-specific PCR (MSP). Loss of A allele and/or hypermethylation were significantly associated with abnormal expression of the A antigen in cases undergoing TUR ($P=0.02$) and radical cystectomy ($P=0.0005$). For the analysis of the concomitant dysplasia in 23 cases with TCC of the bladder, the expression of the A antigen was maintained, regardless of the A allelic loss or methylation status in the tumor. In conclusion, A allelic loss and hypermethylation in the promoter region of the *ABO* gene showed significant correlation with reduction of A antigen expression in TCC, while the expression of the A antigen is maintained in concomitant dysplasia or normal urothelium, suggesting that loss of the *ABO* gene and/or its promoter hypermethylation is a specific marker for TCC.**
*Laboratory Investigation* (2005) **85,** 895–907. doi:10.1038/labinvest.3700268; Published online 9 May 2005

**Keywords:** bladder cancer; *ABO* gene; LOH; promoter hypermethylation; dysplasia

Superficial bladder cancers often show multifocal occurrences or metachronous recurrence after transurethral resection (TUR), and eventually develop into invasive bladder cancer. Allelic loss on chromosome 9 is the most frequent genetic event in transitional cell carcinomas of the bladder,[1–4] that is observed in 70% of invasive bladder cancers and even in 50% of superficial bladder cancers at Stage G1.[4] Whether or not loss on chromosome 9 arises in urothelial lesions such as dysplasia is crucial to the understanding of early genetic events in bladder carcinogenesis. Some authors have reported on the allelic loss of chromosome 9 that occurs in the small urothelial lesions and normal bladder urothelium in their attempts to trace genetic alterations using microsatellite markers.[5,6] However, it is still difficult to analyze allelic status in small epithelial regions obtained from formalin-fixed, paraffin-embedded tissues, and a few data have been reported regarding early genetic alterations in bladder dysplasia.[3,7] ABO (H) blood group antigens are constitutively expressed on epithelial cells such as those found in the gastrointestinal tract and urothelium. A reduction in blood-group A antigen (GalNAcα1-3[Fucα1-2]Galβ1-3GlcNAc-R) expression was reported in transitional cell carcinoma (TCC) of the bladder

Correspondence: Dr K Sugano, MD, PhD, Oncogene Research Unit/Cancer Prevention Unit, Tochigi Cancer Center Research Institute, 4-9-13 Yohnan, Utsunomiya-shi, Tochigi Pref. 320-0834, Japan.
E-mail: ksugano@tcc.pref.tochigi.jp
Received 16 April 2004; revised 1 January 2005; accepted 14 January 2005; published online 9 May 2005

and showed significant correlation with an invasive phenotype.[8–11] Orntoft and Wolf[12] examined the correlation between blood-group antigen expression and the activity of glycosyltransferases in TCC of the bladder and reported that the activity of A glycosyl transferase was severely reduced in tumors showing loss of A antigen expression. This phenomenon drew our attention, due to the fact that the determinant of the ABO blood-group antigen is synthesized by the action of the *ABO* gene encoding ABO glycosyltransferase assigned to chromosome 9q34.1, where loss of heterozygosity (LOH) was frequently reported in bladder cancer.[1–4] The *ABO* gene is composed of seven exons and six introns and encodes ABO glycosyltransferase, of which substrate specificity is determined by genetic polymorphisms in exons 6 and 7 (Figure 1).[13,14] Blood-group A antigen is synthesized by α-*N*-acetylgalactosaminyltransferase (A-GalNAc transferase), which catalyzes the transfer of *N*-acetylgalactosamine to the subterminal β-galactosyl residue of the blood-group H carbohydrate chain. Blood-group B-antigen is synthesized by B-galactosyl transferase, which catalyzes the transfer of galactose to the subterminal β-galactosyl residue of the blood-group H carbohydrate chain. The *ABO* gene in blood-group O donors lacks glycosyltransferase activity, for it has a deletion on a guanine residue at the nucleotide position 261 in exon 6, causing protein truncation at codon 117.[13–16] Immunohistochemistry using anti-A monoclonal antibody in bladder cancer may be useful to evaluate the allelic status of the *ABO* gene locus at 9q34.1 in those who are heterozygous for ABO genotypes. Expression of blood-group A antigen is stable enough even in formalin-fixed paraffin-embedded specimens, and this could be applicable in the analysis of small lesions that are too small to be examined by genetic analysis. Two papers were so far reported as to the correlation between reduced expression of A antigen and A allelic loss in TCCs of the bladder.[17,18] Meldgaard *et al*[17] analyzed 22 bladder tumors for LOH of the 9q allele by PCR-restriction fragment length polymorphism (RFLP) analysis of the *ABO* locus at 9q34. Seven tumors from heterozygous informative individuals were sorted by flowcytometry. LOHs were detected in the most aneuploid subpopulation of cells in two cases, but both cases were losing O-alleles. No LOHs were detected in analysis of the low aneuploid subpopulation. As all tumors showed loss of blood group ABH antigen expression, they concluded that LOH of the *ABO* locus on chromosome 9q34 is not the cause of loss of blood group ABH expression in human bladder cancer.[17] Orlow *et al*[18] analyzed 19 patients with bladder cancer serologically typed as blood group A. Expression of A antigen was maintained in 14 samples in normal urothelium, while it was reduced in nine tumors. PCR-RFLP analysis showed loss of the A allele in one tumor sample showing reduced expression of the A antigen. They indicated that the lack of the A antigen expression in certain bladder tumors is due to the allelic loss of the *ABO* gene and that in some of these tumors, the loss involved the surrounding chromosomal region at 9q34.1–4.[18] These two reports did not support the correlation between A-allelic loss and the reduced expression of the A antigen in the majority of bladder cancers. Recent advance in cancer epigenetics shed light on the reduced expression of A antigen in malignant cells. Kominato *et al*[19,20] reported that hypermethylation of the promoter region of the *ABO* gene induced *ABO* gene silencing in their study using a human stomach carcinoma cell line. Iwamoto *et al*[21] established subclones with positive or negative expression of the A antigen from parental colonic cancer cell lines and reported a distinct difference in the methylation pattern of the CpG island of the promoter region of the ABO glycosyltransferase, that is densely methylated in a subclone lacking the expression of the A antigen. Gao *et al*[22] examined 30 oral squamous carcinomas for expression of the A and B antigens and A/B glycosyltransferase, together with LOH at the *ABO* locus and hypermethylation of the *ABO* gene promoters. Loss of A or B antigen expression was found in 21 of 25 tumors (84%), while the expression of the glycosyltransferase was absent in all of tumors showing negative expression of A or B antigens. Loss of the A or B allele was found in 3/20 tumors (15%) heterozygous for the *ABO* locus and hypermethylation of the promoter region in 10 of 30 tumors (33.3%).[22] Furthermore, Habuchi *et al*[23] reported that the region 9q32–9q33, which is in the vicinity of the *ABO* gene locus at 9q34.1, is a frequent target of LOH and methylation in bladder cancer. These findings prompted us to hypothesize that deletion of blood-group A antigen expression in TCC of the bladder might be regulated by a combination of genetic and epigenetic mechanisms, that is, an LOH of the *ABO* gene locus and hypermethylation of the *ABO* gene promoter region. The purpose of this study was to elucidate the relevant mechanisms underlying the loss of blood group A antigen expression in TCC of the bladder and whether it could be used as a phenotypic marker to estimate any underlying genetic and epigenetic abnormalities in normal urothelium and concomitant bladder dysplasia in patients with bladder cancer.

## Materials and methods

### Samples and DNA Extraction

A total of 81 cases of TCC of the bladder were studied, of which 44 underwent TUR and 37 underwent radical cystectomy (Table 1). The histo-blood group for all cases was A (72 cases) or AB (nine cases) examined by routine hemagglutination tests at hospital. Tumors were graded and staged according to the WHO classification or the 1997 UICC TNM classification system. Based on patients'

**Table 1** Patient background

| | *TUR-BT* | *Radical cystectomy* | P-*value* |
|---|---|---|---|
| No. of cases examined | 44 | 37 | |
| *Gender* | | | NS |
| Male | 37 (84.1%) | 33 (89.2%) | |
| Female | 7 (15.9%) | 4 (10.8%) | |
| Age (median) | 66 (45–79) | 66 (39–89) | NS |
| *Pathological stage* | | | $P<0.01$ |
| pTa | 14 (31.8%) | 0 (0%) | |
| pT1 | 25 (56.8%) | 11 (29.8%) | |
| pT2 | 4 (9.1%) | 8 (21.6%) | |
| pT3 | 0 (0%) | 10 (27.0%) | |
| pT4 | 1 (2.3%) | 8 (21.6%) | |
| *Hitological grade* | | | $P<0.01$ |
| G1 | 7 (14.9%) | 0 (0%) | |
| G2 | 21 (51.1%) | 2 (5.4%) | |
| G3 | 16 (34.0%) | 35 (94.6%) | |
| *Blood group* | | | |
| A | 38 | 34 | |
| AB | 6 | 3 | |

history, the proportion of cases with advanced stage or high-grade tumors was significantly higher in those who underwent radical cystectomy than those who underwent TUR ($P<0.01$). In 44 patients who underwent TUR, DNA was extracted from fresh specimens and normal DNA was extracted from peripheral blood lymphocytes (PBL) by a standard procedure using proteinase K digestion followed by phenol–chloroform extraction. In 37 cases that underwent radical cystectomy, a total of 1130 paraffin-embedded specimens obtained from mapping study of the bladder were histologically confirmed by hematoxylin and eosin staining as being composed of tumor, dysplasia and normal tissues. DNA was extracted from manually dissected tumors and corresponding normal tissues using DEXPAT (TAKARASHUZO Co., Ltd, Shiga, Japan) according to the manufacturer's recommendation.

### Expression of Blood-Group A Antigen by Immunohistochemical Staining

In all, 4-$\mu$m-thick sections from formalin-fixed, paraffin-embedded specimens of resected tissues that underwent TUR or radical cystectomy were used for immunohistochemical staining (IHC). A mapping study of the bladder specimens revealed concomitant dysplastic lesions in 23 cases that underwent radical cystectomy, and they were then subjected to IHC performed as described previously.[24] Mouse monoclonal antibody (mAb) directed against A antigen (clone 81FR2.2; DAKO, Carpinteria, CA, USA) was used as the primary antibody and the avidin–biotin-conjugated immunoperoxidase technique was performed with a DAKO LSAB2 Kit (DAKO, Carpinteria, CA, USA). Reportedly, the specificity of the mAb 81FR2.2 was characterized by transfection experiment of the A-glycosyl transferase gene to the HeLa cell (genotype OO).[25] Erythrocytes, normal epithelium and vascular endothelium were used as internal positive controls, while muscle and connective tissues served as negative controls. To determine the specificity of A antigen, IHC was performed for normal urothelium of blood group B and O donors. Immunohistochemistry for A antigen was classified as follows: 'negative' if the section had no positively (0%) stained tumor cells, 'positive' if staining was seen across the section (>70% positively stained tumor cells), and 'heterogenous' if <70% of tumor cells stained positively. As to the correlation with A allelic loss or methylation status, cases showing positive or heterogenous expression were compared with those showing negative expression.

### Allelic Status on 9q Loci Defined by Blunt-End Single-Strand DNA Conformation Polymorphism Analysis

LOH of the *ABO* gene locus was examined by blunt-end Single-strand DNA conformation polymorphism (SSCP) analysis,[26] using genetic polymorphisms at nucleotide positions 261 and 297 in exon 6 of the *ABO* gene. Genotypes and their allelic frequencies in Japanese population were previously reported[15] and shown in Figure 1. Four groups of alleles, A (A101, A102, A103), B (B101, B102, B103, A104), O1 (O101, O102, O202, O203) and O2 (O103, O201) were identified by the analysis of two genetic polymorphisms (nucleotides 261, 297) in exon 6 of the *ABO* gene. The 5′-terminus of the reverse primer

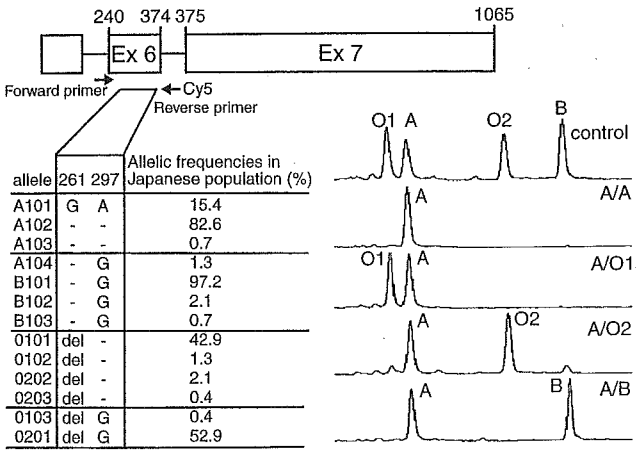


**Figure 1** Schema of single nucleotide polymorphisms (SNPs) in exons 6 of the *ABO* gene and electropherogram of the blunt-end SSCP analysis showing examples of normal DNA from blood group A or A/B donors. SNPs in nucleotide positions 261 and 297 were used for analysis in this study. DNA variants and their allelic frequencies reported in the Japanese are indicated.[15] The blood group *O* gene has a single base deletion at position 261 resulting in a frame-shift mutation and causing protein termination at codon 117.

was labeled with Cy5 flourescent dye. The nucleotide sequences of the forward and reverse primers were 5′-TCTCCATGTGCAGTAGGAAGGATG-3′ and 5′Cy5-ATGGCAAACACAGTTAACCCAATG-3′, respectively. PCR conditions were as follows: 0.5–1.0 μg of genomic DNA as a template, 0.2 μmol/l of each primer, 0.125 mmol/l deoxynucleoside triphosohate (dNTP), 0.25 units of AmpliTaq Gold DNA polymerase (Perkin Elmer-Cetus, Norwalk, CT, USA) in a total reaction volume of 25 μl. After the first denaturation step at 95°C for 12 min, 40 cycles were performed for amplification consisting of 30 s at 95°C, annealing for 30 s at 57°C, and extension for 30 s at 72°C followed by a final extension at 72°C for 7 min. PCR products were then treated with Klenow fragment (TAKARA SHUZO Co., Ltd, Shiga, Japan) to generate DNA fragments with blunt ends. To 1 μl of each PCR product, 0.5 units of Klenow fragment was added, and the mixture was incubated at 37°C for 30 min. One microliter of this reaction mixture was diluted with 10 μl of loading solution (90% deionized formamide, 20 mM EDTA, 0.05% bromophenol blue) and heat denatured at 95°C for 5 min. An ALF red automated DNA sequencer™ (Pharmacia, Tokyo, Japan) was used for blunt-end SSCP analysis. One microliter of the diluted mixture was applied onto a 15% polyacrylamide gel (30:1, acrylamide:bisacrylamide ratio) containing Tris/glycine buffer (25 mM Tris, 192 mM glycine). Electrophoresis was performed at 30 W for 16 h using a continuous buffer system consisting of 25 mM Tris and 192 mM glycine. During electrophoresis, the gel was maintained at a constant temperature of 18°C by a circulating water bath. The data were analyzed using the ALF Win Fragment analyzer 1.02™ software package (Pharmacia, Tokyo, Japan). LOH was determined by measuring the signal ratio between the opposing alleles and defined as tumor cellularity according to the equation that we previously reported.[4,26,27] Supposing that the A1 allele is lost in a heterozygote carrying A1 and A2 alleles, $T$ is the peak height of the signal from the tumor samples and $N$ is the peak height of the signal from normal control. The tumor cellularity in the sample is thus given as follows:

$$\text{Tumor cellularity (\%)} = [(N_{A1}/N_{A2}) - (T_{A1}/T_{A2})]\times 100/(N_{A1}/N_{A2})$$

Genomic DNA from normal PBL was analyzed to set the cutoff values for tumor cellularity. As previously reported, the mean + 3s.d. values of the normal heterozygous DNA were used as a cutoff value for tumor cellularity, and tumor samples showing tumor cellularities above the cutoff level were considered to have LOHs.[4] A104 allele was indistinguishable from B allele in this analysis, while the observed frequency of the A104 allele in the Japanese is reported to be as low as 1.3%. In fact, in all samples tested, the genotypes coincided with the patient's ABO isotypes. In addition, two single base nucleotide polymorphism markers (*ALDOB*, 9q21.3 and *VAV2*, 9q34.1) were used to assess the allelic status on 9q according to the method that we previously reported;[4] the former is centromeric and the latter is telomeric to the *ABO* gene locus, respectively (Figure 4). Nucleotide sequences of the forward and reverse primers for *ALDOB* and *VAV2* were as follows: 5′Cy5-GGGCTTGACTTTC CAACACG-3′ and 5′-TCTAGCCTCAATCCTCATAC-3′ (*ALDOB*), 5′-GTGTCTGCACTGGCCACACT-3′ and 5′Cy5-TCCAAAGGACCTTCTCCAAA-3′ (*VAV2*).

### Bisulfite PCR-SSCP Analysis and Methylation-Specific PCR

In cases that underwent TUR, methylation status in the promoter region of the *ABO* gene was analyzed by bisulfite PCR-SSCP (BiPS) and methylation specific PCR (MSP).[24,28,29] Seven primer sets were designed to amplify seven overlapping regions spanning the CpG island located from −765 to +21 relative to the translation start site (Figure 2). Primer sets *re 1* through *re 6* were designed for BiPS analysis and *RE7*.M and *RE7*.UM were for MSP. Bisulfite treatment was performed using the CpGenome DNA Modification Kit (Intergen Co., New York, NY, USA). In all, 1 μg of tumor-derived DNA was treated with Na-bisulfite according to the manufacturer's recommendations. PCRs were performed in 25 μl reaction volumes containing 10 × buffer, 1.0 μl bisulfite-modified DNA corresponding to 50 ng of genomic DNA as a template, 0.2 μmol/l of each primer, 0.125 mmol/l dNTP and 0.25 units of AmpliTaq Gold DNA polymerase. PCR conditions were 95°C for 9 min for heat denaturation, 40 cycles of 94°C for 1 min, 1 min at the different annealing temperatures for each primer set (Table 2), 72°C for 2 min for amplification, followed by a final extension at 72°C for 10 min. The BiPS procedure was performed as previously described.[28,29] Nondenaturing polyacrylamide gels of 8% for *re 2* and *re 6*, 10% for *re 1*, *re 4* and *re 5*, and 15% for *re 3* were used for the analysis. CpGenome™ Universal Methylated DNA (CHEMICON International, Temecula, CA, USA) was used as a positive control, and PBL obtained from healthy control donors were used as a negative control. When extra bands were observed, they were cut from the gels, reamplified and subjected to direct sequencing using ABI 3100 PRISM sequencer with a Big-Dye terminator sequencing kit (Perkin-Elmer). In analysis of cases that underwent radical cystectomy, BiPS analysis was not employed due to the technical difficulty for reliable amplification of relatively long sized DNA fragments from formalin-fixed paraffin-embedded sections. In cases that underwent radical cystectomy, methylation status was assessed by MSP of region 7, the most proximal to the translation start site. The size of the PCR product was as short as 96 bp and amplifiable from archival samples with

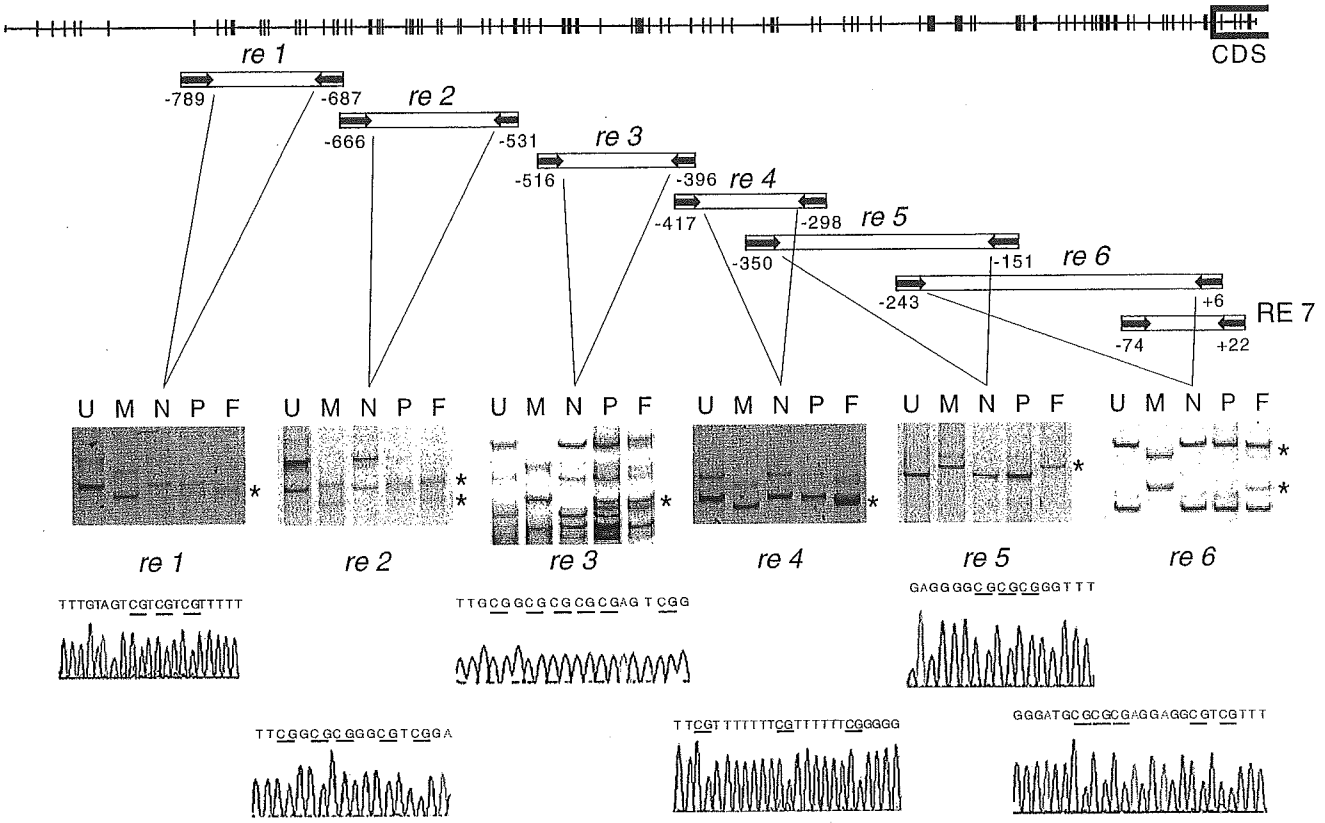


**Figure 2** Map of the 5′ CpG island of the *ABO* gene and result of BiPS analysis. (Top) CpG sites in the promoter region of the *ABO* gene are indicated by vertical lines. (Middle) The amplified DNA fragments from regions 1 to 7 are indicated. PCR primer set of each region was indicated by arrows. (Bottom) BiPS analysis of the *ABO* gene. Extra bands are indicated by asterisks. After SSCP analysis, the extra bands were excised from gels, reamplified by PCR, and sequenced. Results of the direct sequencing of the case with full methylation were shown in the lower panel. U: unmethylated control, M: methylated control, N: no methylation, P: partial methylation, F: full methylation, *extra band showing mobility shift.

**Table 2** Primer sequences for BiPS analysis and MSP

| *Primer name* | *Forward primer sequence* | *Reverse primer sequence* | *Products length (bp)* | *No. of CpG sites* | *Annealing temperature (°C)* |
|---|---|---|---|---|---|
| *re 1* | 5′-TTGGGATTTTTCGGGAGGTAATTT-3′ | 5′-CCCCGCTACGACCCCCGCCCTTAC-3′ | 103 | 11 | 54 |
| *re 2* | 5′-GGGCGGAGCGGGGTTTTGTTTACG-3′ | 5′-CGCGACCCCACGAAACTCTACGTC-3′ | 136 | 20 | 48 |
| *re 3* | 5′-AGCGATTTTGTTTAGGGGGA-3′ | 5′-ACTACGACCCCAAAACCCAC-3′ | 121 | 15 | 59 |
| *re 4* | 5′-TCGTGGGTTTTGGGGTCGTAGTTT-3′ | 5′-CCCCGTCCCCGAAAACCCCTTAAC-3′ | 120 | 11 | 54 |
| *re 5* | 5′-GGGGGTCGTTTTCGTTCGGGAGAT-3′ | 5′-CGAATCCCCAAAAACCCCTACTAA-3′ | 200 | 19 | 48 |
| *re 6* | 5′-TAAGGTATTAGGGTTACGAGG-3′ | 5′-GACCATAACTCCGCGTCTAAT-3′ | 248 | 33 | 49 |
| *RE 7.M* | 5′-GAGGGGGCGTTTCGGGTTTATTTC-3′ | 5′-ACGTCCGCAACACCTCGACCATAA-3′ | 96 | 16 | 70 |
| *RE 7.UM* | 5′-GGAGGGGGTGTTTTGGGTTTA-3′ | 5′-ATCCACAACACCTCAACCATAACT-3′ | 96 | 13 | 60 |

M, methylated; UM, unmethylated.

relative ease; however, five out of 37 cases that underwent radical cystectomy failed in PCR amplification. Methylation status of region 7 was used as the surrogate indicator for extensive methylation of the CpG sites or full methylation.

### Statistical Analysis

Statistical analysis was performed using a likelihood $\chi^2$ analysis or Fisher's exact test. Probability ($P$) values of $<0.05$ were considered to be significant.

## Results

### Expression of the A Antigen in TCC of the Bladder by IHC

Expression of the A antigen in tumor and normal urothelium was examined by IHC (Figure 3A). The corresponding staining of A antigen on the normal

urothelium from histo-blood-group B or O donors resulted in background levels only (data not shown). All of the normal urothelium from blood-group A individuals stained positively. The numbers of cases showing positive, heterogeneous and negative staining were 11 (25.0%), 11 (25.0%) and 22 (50.0%) in 44 tumor specimens that underwent TUR, while they were 14 (37.8%), 5 (13.5%) and 18 (48.6%) in 37 tumor specimens that underwent radical cystectomy. The overall frequencies of negative A antigen

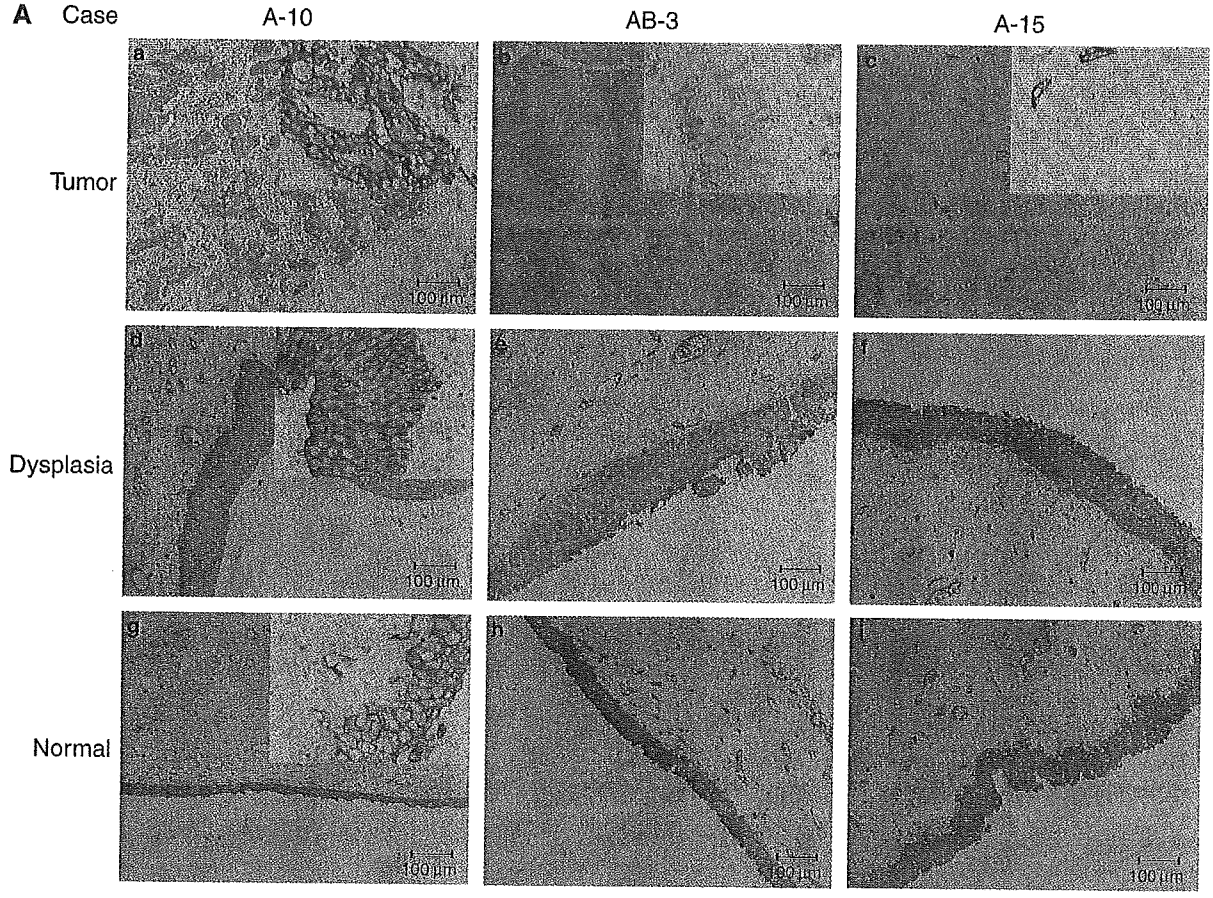


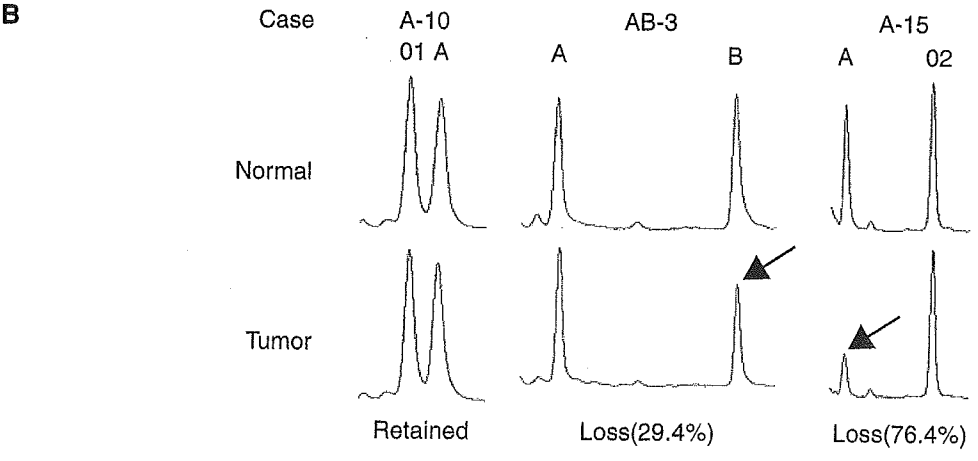


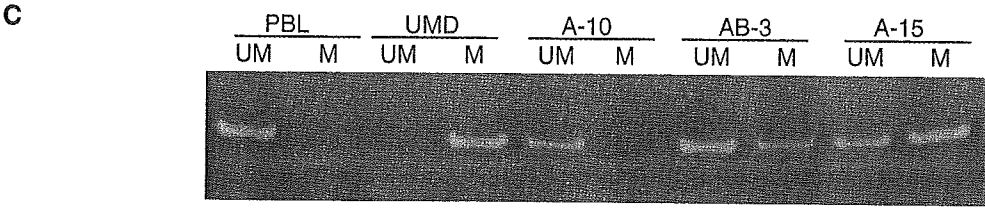

expression were 35.7% (5/14) for pTa, 58.3% (21/36) for pT1, 25.0% (3/12) for pT2, 40.0% (4/10) for pT3 and 77.8% (7/9) for pT4 stages, and 71.4% (5/7), 43.5% (10/23) and 49.0% (25/51) for Grade 1, 2 and 3 tumors, respectively. There were no significant differences between A antigen expression and tumor stages or histological grades.

### LOH on 9q in TCC of the Bladder

Allelic status of the *ABO* gene and neighboring loci were analyzed by blunt-end SSCP analysis using three polymorphic markers (*ABO* (9q34.1), *ALDOB* (9q21.3-22.2), *VAV2* (9q34.1)) (Figure 4). Heterozygosity of each locus was 87.7% (71/81) for *ABO*, 52.6% (41/78) for *ALDOB* and 48.1% (38/79) for *VAV2*, respectively. As all samples were derived from patients with an A or AB blood group, heterozygosity at the *ABO* locus was highest of all the loci examined. Genotypes of the *ABO* gene were classified into four groups, that is, A/A ($n=10$), A/O1 ($n=34$), A/O2 ($n=26$) and A/B ($n=9$). The cutoff value for tumor cellularity in each genotype was defined as the mean + 3s.d. of the normal DNA samples: 20% for A/O1, 22% for A/O2, 26% for A/B, respectively. In 44 cases that underwent TUR, frequencies of LOH were 53.7% (22/41) for *ABO*, 43.5% (10/23) for *ALDOB* and 50.0% (10/20) for *VAV2*, respectively. Frequencies of allelic loss at the *ABO* locus were 23.1% (9/39), 33.4% (6/18), 33.3% (5/15) and 33.3% (2/6) for A, O1, O2 and B allele, respectively. In 37 cases that underwent radical cystectomy, frequencies of LOH were 76.7% (23/30) for *ABO*, 77.8% (14/18) for *ALDOB* and 83.3% (15/18) for *VAV2*, respectively. Frequencies of allelic loss in the *ABO* locus was 23.3% (7/30), 50.0% (8/16), 54.5% (6/11) and 66.7% (2/3) for A, O1, O2 and B allele, respectively. There were no significant differences as to the frequencies of LOH between three markers and between four alleles of the *ABO* gene. Frequencies of LOH were higher in cases that underwent radical cystectomy as compared to the TUR cases, that is, 76.7% (23/30) *vs* 53.7% (22/41) for *ABO* ($P=0.08$), 77.8% (14/18) *vs* 43.5% (10/23) for *ALDOB* ($P=0.054$) and 83.3% (15/18) *vs* 50.0% (10/20) for *VAV2* ($P=0.043$), among which VAV2 locus showed statistical significance.

### Methylation Status of the *ABO* Gene Promoter Region

CpG island of the *ABO* gene extends from 0.7 kb upstream to 0.6kb downstream from the translation start site in exon 1. Reportedly, the promoter region of the *ABO* gene is located between −117 and +31 from the translation start site, of which hypermethylation regulates gene expression.[19,20] In the present study, we divided CpG island spanning −789 to +6 into six regions and examined the methylation status by BiPS analysis (Figure 2). In the preliminary experiment, methylated DNA could be identified as the extra band, if more than 25% of the template DNA was methylated (data not shown). Methylation patterns were defined as follows: full methylation if all regions showed methylation, partial methylation if at least one region showed methylation and no methylation. A total of 44 TUR cases were analyzed, and we assessed the correlation between methylation status and expression levels of the A antigen using a panel of 35 cases, for nine cases showing LOH of the A allele were not included in the first assessment (Tables 3 and 4). Frequencies of methylation in *re 1* through *re 6* were 17.1% (6/35), 28.6% (10/35), 34.3% (12/35), 11.4% (4/35), 14.3% (5/35) and 11.4% (4/35), respectively (Table 4). In *re 4*, *re 5* and *re 6*, methylation was not detected in all cases showing positive or heterogenous expression and expression of the A antigen was negative in four cases showing full methylation. Frequencies of cases showing negative A antigen expression were 100% (4/4) in full methylation, 66.7% (6/9) in partial methylation and 27.3% (6/22) in no methylation and significant association was observed between methylation status (full, partial and no methylation) and expression of the A antigen ($P=0.0093$) (Table 4). In analysis using MSP, methylation of *RE 7* was observed in nine cases, of which six cases showed full or partial methylation in BiPS analysis and the expression of the A antigen was negative in these six cases (Table 3). Discrepancies between MSP and BiPS analysis were shown in three cases, which showed methylation only in MSP and heterogeneous expression of the A antigen. Positive expression of the A antigen was found in 11 cases, in which two cases showed methylation of regions 1 through 3 by BiPS analysis and no cases showed methylation of *RE 7* by MSP (Table 3).

### Correlation of the Expression of A Antigen with A Allelic Loss and Hypermethylation of the *ABO* Gene Promoter Region

In analysis of 44 cases that underwent TUR, loss of the A allele was observed in nine cases, among

**Figure 3** Expression of the blood-group A antigen, allelic status of the *ABO* gene and MSP of region 7 in cases that underwent radical cystectomy. (**A**) Immunostaining of A antigen in tumor (a, b, c), dysplasia (d, e, f), and corresponding normal urothelium (g, h, I) from cases A-10, AB-3 and A-15, respectively. A-10 showed positive staining in tumor (a), dysplasia (d) and normal urothelium (g), while the tumor section showed heterogeneous staining for the case AB-3 (b), and negative staining for the case A-15 (c). Normal urothelium from cases A-10 (g), AB-3 (h) and A-15 (i) stained positively. Reduced from × 100. High magnification view ( × 400) was shown as inset. (**B, C**) Analysis of LOH of the *ABO* gene locus using blunt-end SSCP and methylation status by MSP (*RE 7*). A-10 showed the expression of the A antigen in tumor tissue, no allelic loss and unmethylated CpG sites. AB-3 showed heterogenous expression of the A antigen and methylation of the *ABO* gene, while the A allele was retained. A-15 showed negative expression of the A antigen, loss of A alleles and methylation of the *ABO* gene.

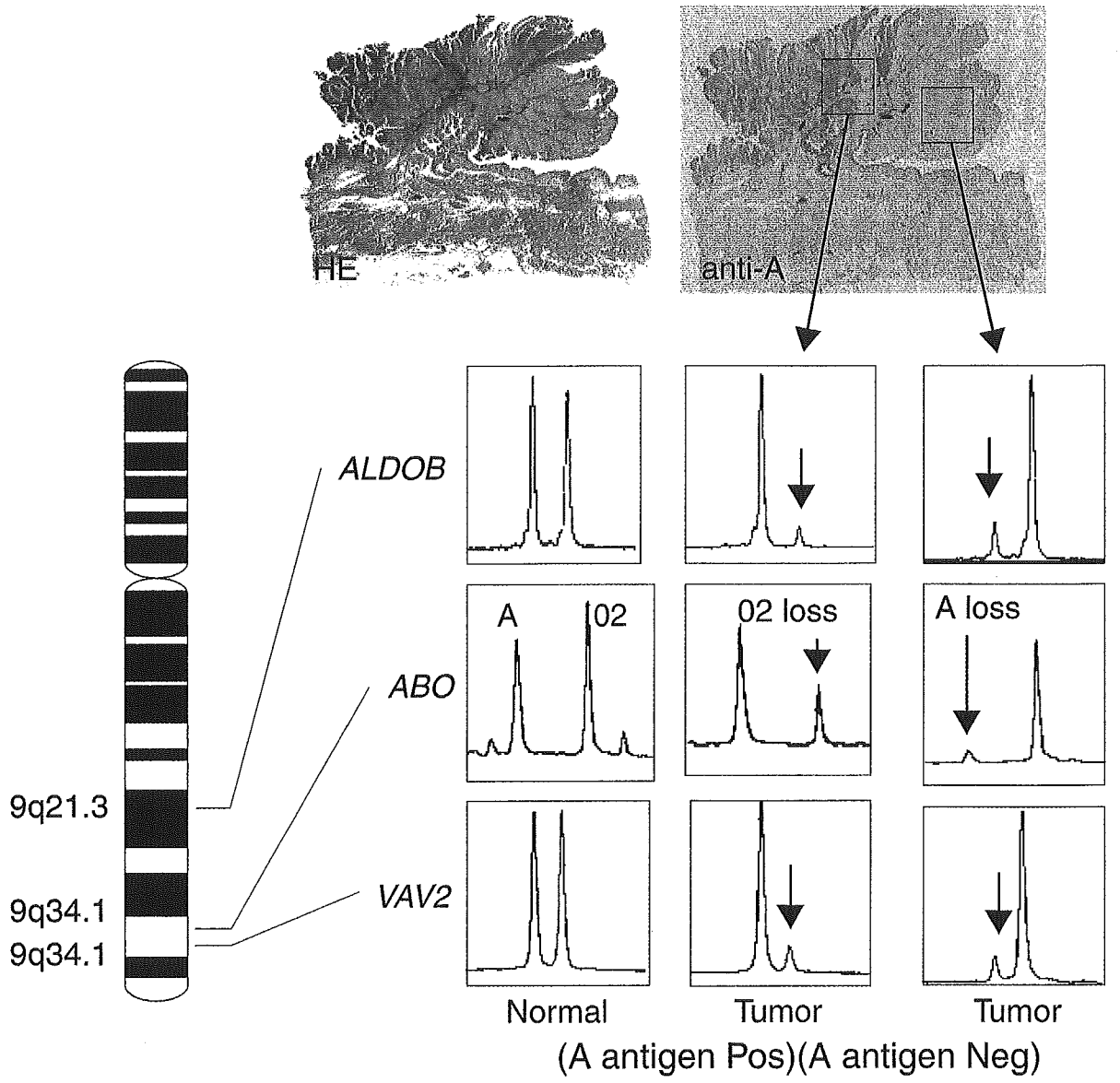


**Figure 4** A case of bladder cancer showing chimeric expression of the A antigen. DNA was extracted from areas showing positive or negative A antigen expression and subjected to blunt-end SSCP analysis using three single nucleotide polymorphic markers (*ALDOB*, *ABO* and *VAV2*) on 9q. The patient's genotype was A/O2. A allele was lost in the sample taken from the area showing negative A antigen expression, while O2 allele was lost in the sample taken from the area showing positive A antigen expression. Note that two polymorphic loci (*ALDOB*, 9q21.3 centromeric to the *ABO* locus and *VAV2*, 9q34.1 telomeric to the *ABO* locus) also showed LOH and suggested a large regional chromosome deletion, while the parental origin of the lost allele in these two loci was different between areas showing A-antigen positive or negative expression.

which six cases showed negative and three cases showed heterogenous expression of the A antigen (Table 5). Cases homozygous for A allele were regarded as retaining at least one copy of the *ABO* gene. No statistical association was found between the expression level of the A antigen and A allelic loss ($P=0.26$). In BiPS analysis, expression of the A antigen was negative in all of the four cases with full methylation and statistical association was shown between the expression of the A antigen and methylation status ($P=0.035$). Taking A allelic loss or full methylation in combination, 76.9% (10/13) cases with A allelic loss and/or full methylation showed negative A antigen expression, while the expression of the A antigen was negative in 38.7% (12/31) of cases that retained A allele and showed partial or no methylation. Cases with A allelic loss and/or full methylation showed significant correlation with negative A antigen expression ($P=0.02$) (Table 5). In analysis of 37 cases that underwent radical cystectomy, A allelic loss was observed in seven cases and they all showed negative A antigen expression in the tumor (Table 6). Compared with 30 cases that retained the A allele (including A/A

**Table 3** Methylation status in the *ABO* gene promoter region and expression of A antigen

| *No.* | *Case* | *Genotype* | *LOH*[a] | *Methylation status*[b] | *Methylation status (%)*[c] | | | | | | *RE 7*[d] | *Expression of A antigen* |
|---|---|---|---|---|---|---|---|---|---|---|---|---|
| | | | | | *re* 1 | *re* 2 | *re* 3 | *re* 4 | *re* 5 | *re* 6 | | |
| 1 | 37 | A/O2 | O2 | Full | +(100) | +(100) | +(100) | +(100) | +(100) | +(71) | + | − |
| 2 | 65 | A/B | B | Full | +(100) | +(100) | +(100) | +(86) | +(100) | +(97) | + | − |
| 3 | 72 | A/O1 | O1 | Full | +(70) | +(62) | +(85) | +(57) | +(87) | +(61) | + | − |
| 4 | 228 | A/B | Ret | Full | +(100) | +(100) | +(100) | +(100) | +(100) | +(100) | + | − |
| 5 | 85 | A/O1 | O1 | Partial | − | +(85) | +(69) | − | +(100) | +(100) | + | − |
| 6 | 235 | A/O1 | O1 | Partial | − | +(85) | +(100) | − | − | − | + | − |
| 7 | 10 | A/O2 | Ret | Partial | − | − | +(23) | − | − | − | − | − |
| 8 | 186 | A/O2 | Ret | Partial | − | +(62) | +(38) | − | − | − | − | − |
| 9 | 220 | A/O1 | O1 | Partial | − | − | +(62) | − | − | − | − | − |
| 10 | 229 | A/O1 | O1 | Partial | − | − | +(46) | − | − | − | − | − |
| 11 | 226 | A/O2 | Ret | Partial | − | − | +(62) | − | − | − | − | +/− |
| 12 | 40 | A/O1 | Ret | Partial | +(100) | +(100) | +(100) | − | − | − | − | + |
| 13 | 141 | A/O2 | O2 | Partial | +(100) | +(100) | +(100) | − | − | − | − | + |
| 14 | 5 | A/O2 | O2 | No | − | − | − | − | − | − | − | − |
| 15 | 43 | A/O1 | O1 | No | − | − | − | − | − | − | − | − |
| 16 | 77 | A/O2 | O2 | No | − | − | − | − | − | − | − | − |
| 17 | 97 | A/O2 | O2 | No | − | − | − | − | − | − | − | − |
| 18 | 195 | A/O1 | Ret | No | − | − | − | − | − | − | − | − |
| 19 | 7 | A/A | NI | No | − | − | − | − | − | − | − | − |
| 20 | 71 | A/B | B | No | − | − | − | − | − | − | + | +/− |
| 21 | 184 | A/O2 | O2 | No | − | − | − | − | − | − | + | +/− |
| 22 | 183 | A/B | Ret | No | − | − | − | − | − | − | + | +/− |
| 23 | 212 | A/O2 | Ret | No | − | − | − | − | − | − | − | +/− |
| 24 | 225 | A/B | Ret | No | − | − | − | − | − | − | − | +/− |
| 25 | 3 | A/A | NI | No | − | − | − | − | − | − | − | +/− |
| 26 | 98 | A/A | NI | No | − | − | − | − | − | − | − | +/− |
| 27 | 78 | A/O2 | Ret | No | − | − | − | − | − | − | − | + |
| 28 | 79 | A/O2 | Ret | No | − | − | − | − | − | − | − | + |
| 29 | 94 | A/O1 | Ret | No | − | − | − | − | − | − | − | + |
| 30 | 185 | A/O2 | Ret | No | − | − | − | − | − | − | − | + |
| 31 | 193 | A/B | Ret | No | − | − | − | − | − | − | − | + |
| 32 | 221 | A/O1 | Ret | No | − | − | − | − | − | − | − | + |
| 33 | 222 | A/O2 | Ret | No | − | − | − | − | − | − | − | + |
| 34 | 45 | A/A | NI | No | − | − | − | − | − | − | − | + |
| 35 | 80 | A/A | NI | No | − | − | − | − | − | − | − | + |

[a]The cases in which A allele was retained were shown.

[b]Full methylation indicates all the regions were methylated, Partial; at least one regions were methylated, No; all the regions were ummethylated by SSCP analysis.

[c]Numbers in parentheses indicate the proportion of CpG sites methylated in the amplified DNA fragments.

[d]Methylation was analyzed using MSP.

**Table 4** Correlation of the expression of A antigen with methylation status in 35 cases underwent TUR

| *Expression of A antigen* | *Each locus (Nos. methylated/nos. unmethylated)* | | | | | | *All loci* | | | P |
|---|---|---|---|---|---|---|---|---|---|---|
| | *re* 1 | *re* 2 | *re* 3 | *re* 4 | *re* 5 | *re* 6 | *Full* | *Partial* | *None* | |
| Positive/Hetero | 2/17 | 2/17 | 3/16 | 0/16 | 0/16 | 0/16 | 0 | 3 | 16 | 0.0093 |
| Negative | 4/12 | 8/8 | 9/7 | 4/12 | 5/11 | 4/12 | 4 | 6 | 6 | |

Among 44 cases that underwent TUR, nine cases showing loss of A allele were not included in Table 4.
Hetero: heterogenous expression.

homozygotes), the frequency of A antigen expression was significantly low in those showing A allelic loss ($P=0.003$) (Table 6). MSP of *RE 7* showed methylation in seven cases (18.9%) in which the expression of the A antigen was negative in six cases. Methylation status was significantly correlated with negative expression of the A antigen ($P=0.03$). Taking A allelic loss and methylation in combination, 91% (10/11) of cases with A allelic loss and/or methylation were negative for the A antigen expression, while the expression of the A antigen was negative in 23.8% (5/21) of cases

**Table 5** Correlation of the expression of A antigen with A alleleic loss and hypermethylation of the *ABO* gene promoter region in 44 cases that underwent TUR

| *Expression of A antigen* | *A allele* | | P | *Full methylation* | *Partial or no methylation* | P | *A loss and/or full methylation*[a] | *A retained and partial/ no methylation* | P |
|---|---|---|---|---|---|---|---|---|---|
| | *Loss* | *Retain* | | | | | | | |
| Positive/ Hetero | 3 | 19 | 0.26 | 0 | 22 | 0.035 | 3 | 19 | 0.02 |
| Negative | 6 | 16 | | 4 | 18 | | 10 | 12 | |

[a]The cases that showed loss of A allele and/or full and partial methylation.
Hetero: heterogenous expression.

**Table 6** Correlation of the expression of A antigen with A allele loss and/or hypermethylation of the *ABO* gene promoter region in 37 cases that underwent radical cystectomy

| *Expression of A antigen* | *A allele* | | P | *MSP (RE 7)* | | P | *A loss and/or methylated* | *A retain and unmethylated* | P |
|---|---|---|---|---|---|---|---|---|---|
| | *Loss* | *retain* | | *M* | *UM* | | | | |
| Positive/heterogenous | 0 | 19 | 0.003 | 1 | 16[a] | 0.03 | 1 | 16 | 0.0005 |
| Negative | 7 | 11 | | 6 | 9[b] | | 10 | 5 | |

[a]Two cases were not available.
[b]Three cases were not available.
M, methylated; UM, unmethylated.

showing retained A allele and no methylation. A allelic loss and methylation were significantly correlated with the expression level of the A antigen ($P=0.0005$) (Table 6). In one case, the expression of the A antigen was chimeric and the tumor was divided into areas showing positive or negative expression (Figure 4). This case was an A/O2 heterozygote, and the allelic status was determined from the dissected specimen. O2 allele was lost in the area showing positive staining, while the A allele was lost in the area showing negative staining. Allelic status was also examined in the *ALDOB* and *VAV2* loci, where the parental origin of the lost allele was different between positively and negatively stained areas, indicating that allelic loss in the tumor involved large chromosomal region between 9q21.3 and 9q34.1.

### Expression of the A Antigen in Dysplasia and Normal Urothelium

A total of 23 cases that underwent radical cystectomy were examined for expression of the A antigen in concomitant dysplastic lesions and normal urothelium (Table 7). In analysis of 13 cases showing positive A antigen expression in the tumor, A allele was retained in all cases and only one case showed hypermethylation together with normal expression of the A antigen in the dysplasia specimen. In analysis of 10 cases showing negative expression of the A antigen in the tumor, eight showed A allelic loss and/or methylation. Abnormal expression of the A antigen was observed only in one case (A-9), in which dysplasia specimen showed heterogeneous expression but A allelic loss and methylation were not observed in the tumor.

## Discussion

Previously, we reported that LOH on chromosome 9 was a frequent genetic event in TCCs of the bladder and its detection in urine samples would be an useful indicator for tumor recurrence in patients with TCC that underwent TUR.[4] Frequencies of LOH of the *ABO* locus examined in this study seems higher than those reported previously.[17,18] In previous studies, allelic status of the *ABO* gene was examined by PCR/RFLP; however, LOH is barely detectable by PCR/RFLP if the proportion of tumor cells in the sample is below 60%, due to the formation of heteroduplex dimers that are resistant to the restriction enzyme digestion.[30] Blunt-end SSCP analysis is a sensitive method to detect an LOH from clinical samples, of which the proportion of tumor cells is as low as 10–20%.[26] However, LOH study from small lesions such as concomitant dysplasia was still difficult due to technical problems. Slebos *et al*[31] reported that the lower the amount of DNA in the PCR, the greater the risk for allele ratios that were abnormal due to a chance distribution of alleles in the reaction and the DNA equivalent of a minimum of about 100 cells is required for a full representation of both alleles in the analysis. Furthermore, DNAs extracted from formalin-fixed paraffin-embedded sections often harbor degradation and fail in the PCR amplifica-